

Next Generation Anodes for Lithium-Ion Batteries

Third Quarter Progress Report 2018

Dennis Dees, Point-of-Contact

Argonne National Laboratory
9700 South Cass Avenue
Argonne, IL 60439
Phone: (630) 252-7349
E-mail: dees@anl.gov

Brian Cunningham, DOE-EERE-VTO Technology Manager

U.S. Department of Energy, Battery R&D
Phone: (202) 287-5686
E-mail: brian.cunningham@ee.doe.gov

Table of Contents

Overview (page 2)

1. Research Facilities Support (page 5)

CAMP Facility Support Activities (ANL) (page 5)

Surface Chemistry on the Oxide Shell and its Impact on Silicon-Based Battery Anodes (ORNL) (page 8)

Thermodynamic Understanding and Abuse Performance (SNL) (page 11)

Hydro/Solvothermal Synthesis and Scale-up of Silicon and Silicon-containing Nanoparticles (ANL) (page 13)

2. Characterization, Diagnostics, and Analysis (page 14)

Lithium Silicate Formation Investigated by FTIR (ORNL) (page 15)

Inherent Reactivity Studies of Lithium Silicides (ANL) (page 16)

Effect of High-Energy Ball Milling on the Electrochemical Performance of Silicate-Coated Silicon Nanoparticles (ANL) (page 19)

Operando Quantification of Lithiation-Delithiation Behavior of Silicon-Graphite Composite Electrodes for Lithium-Ion Batteries (ANL) (page 21)

3. Materials Advancements (page 23)

Critical Role of Supporting Materials for Silicon Lithium-Ion Batteries (ANL) (page 23)

Probe the Relationships between Functional Electrolytes Structure and SEI Property for Si Materials (LBNL) (page 25)

Silicon Surface Modification and Interaction (NREL) (page 27)

Interfacial Modification of Si Anode for High Energy Li-ion Battery (ANL) (page 30)

Development of High Energy Metals (LBNL) (page 33)

Si Anodes with Extended Cycle Life and Calendar Life (PNNL) (page 35)

Lithium Inventory (ANL) (page 37)

Silicon Deep Dive Overview

Project Introduction

Silicon has received significant attention as a viable alternative to graphitic carbon as the negative electrode in lithium-ion batteries due to its high capacity and availability [1]. Elemental silicon can theoretically store >3500 mAh/g, nearly an order of magnitude higher than graphite (372 mAh/g and 818 mAh/mL, respectively). However, several problems have been identified that limit its utility including large crystallographic expansion (~320%) upon lithiation which translates to particle cracking, particle isolation, and electrode delamination issues. Further, there are fundamental and volume change related SEI stability issues, which affect cycling efficiency. The wealth of previous studies in this area is both a testament to its potential and the size of the challenge that must be overcome, requiring a great amount of innovation on multiple fronts.

BatPaC [2], a techno-economic program designed to model lithium-ion battery performance and cost, was utilized to establish program relevance by connecting DOE/USABC pack performance targets to anode targets. Generally, research with silicon containing anodes is focused on improving the specific capacity of graphite. However, this simple metric requires a more detailed analysis with factors such as the impact on average cell voltage, and volumetric capacity. It is notoriously difficult to select appropriate metrics that will enable an accurate calculation of the energy of a single electrode. Most methods estimate the volumetric energy density of active materials with the simplistic assumption that bulk density of the electrode does not undergo change in volume during cycling. While this serves well for most cathodes where the voltage can be fixed against lithium it is inappropriate for electrodes such as silicon.

As shown in Figure 1 (left frame), BatPaC calculations indicate anode volumetric capacities greater than 1000 mAh/cm³ ($= \rho \cdot \epsilon \cdot Q$ [g/cm³_{act} · cm³_{act}/cm³_{elect} · mAh/g]) generally minimizes battery cost with an advanced NMC cathode. Note that higher capacities result in diminishing savings in cost. The analysis (right frame) also predicts that silicon-graphite electrodes with less than 75 wt% graphite can achieve the target. Finally, alloys of inactive metals (not shown) with silicon (or tin) can meet the volumetric capacity target as long as the metal choice is inexpensive (e.g. iron rather than nickel or cobalt).

Next Generation Anodes for Lithium-Ion Batteries, also referred to as the Silicon Deep Dive Program, is a five National Laboratory consortium assembled to tackle the barriers associated with development of an advanced lithium-ion negative electrode based upon silicon as the active material. This research program baselines promising silicon materials that can be developed or obtained in quantities sufficient for electrode preparation within the consortium facilities. Composite electrode and full cell development leverages recent investments made by DOE-EERE-VTO in electrode materials and characterization. The primary objective of this program is to understand and eliminate the barriers to implementation of a silicon based anode in lithium-ion cells. The Labs are focused on a single program with continuous interaction, clear protocols for analysis, and targets for developing both the understanding and cell chemistry associated with advanced negative electrodes for lithium-ion cells. First and foremost, this undertaking is a full electrode/full cell chemistry project leveraging baseline electrodes prepared at the consortium facilities. All efforts are directed to understanding and developing the chemistry needed for advancing silicon-based anodes operating in full cells. Materials development efforts include active material development, binder synthesis, coatings, safety, and electrolyte additives. Efforts include diagnostic research from all partners, which span a wide range of electrochemical, chemical and structural characterization of the system across length- and time-scales. Specialized characterization techniques developed with DOE-EERE-VTO funding, include neutrons, NMR, optical, and X-ray techniques being employed to understand operation and failure mechanisms in silicon-based anodes. In addition, several strategies to mitigate lithium loss are being assessed. The project is managed as a single team effort spanning the Labs, with consensus decisions driving research directions and toward development of high-energy density lithium-ion batteries.

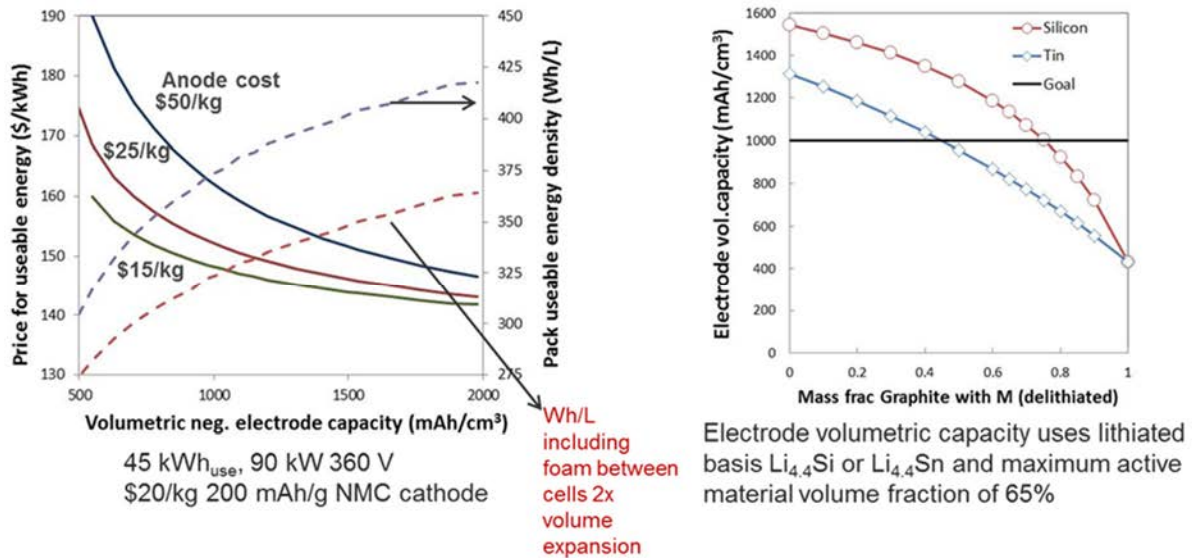


Figure 1. Battery Performance and Cost (BatPaC) model utilized to establish relevance by connecting pack to anode targets.

Objectives

- Understand and overcome the science and technology barriers to the use of silicon-based anodes in high-energy density lithium-ion batteries for transportation applications.
 - Stabilize the SEI
 - Stabilize the electrode
- Demonstrate functional prototype lithium-ion cell chemistries which meet the DOE/USABC performance targets.

Approach

Sandia National Laboratories (SNL), Oak Ridge National Laboratory (ORNL), National Renewable Energy Laboratory (NREL), Pacific Northwest National Laboratory (PNNL), Lawrence Berkeley National Laboratory (LBNL), and Argonne National Laboratory (ANL) have teamed together to form an integrated program. Technical targets have been developed and regular communications have been established. Throughout the program, there is a planned focus on understanding, insights into, and advancement of silicon-based materials, electrodes, and cells. All anode advancements will be verified based on life and performance of full cells. Toward that end, baseline silicon-based materials, electrodes, and cells have been adopted, along with full cell testing protocols.

In examining improvements, changes to the baseline cell technology will be minimized. As an example, silicon active material coating improvements will be verified on baseline silicon materials in electrodes fabricated by the battery research facilities. All other components in the prototype cells (i.e. positive electrode, separator, electrolyte ...) will be from the baseline technology. There are many testing protocols that can be utilized to benchmark the baseline technology. This program has adopted a testing protocol from the literature [3] that has worked well for lithium-ion cells with silicon containing anodes. Shown pictorially in Figure 2 the test starts with three slow ($C/20$) formation cycles, an HPPC cycle, and then the $C/3$ aging cycles. The test ends with another HPPC cycle and three more slow ($C/20$) cycles. All constant current cycling is symmetric between charge and discharge rates. The tests are run at 30°C . If there is little or no aging in the first 100 cycles, the protocol can be repeated. This protocol effectively examines capacity, impedance, and aging effects in about a month's worth of testing.

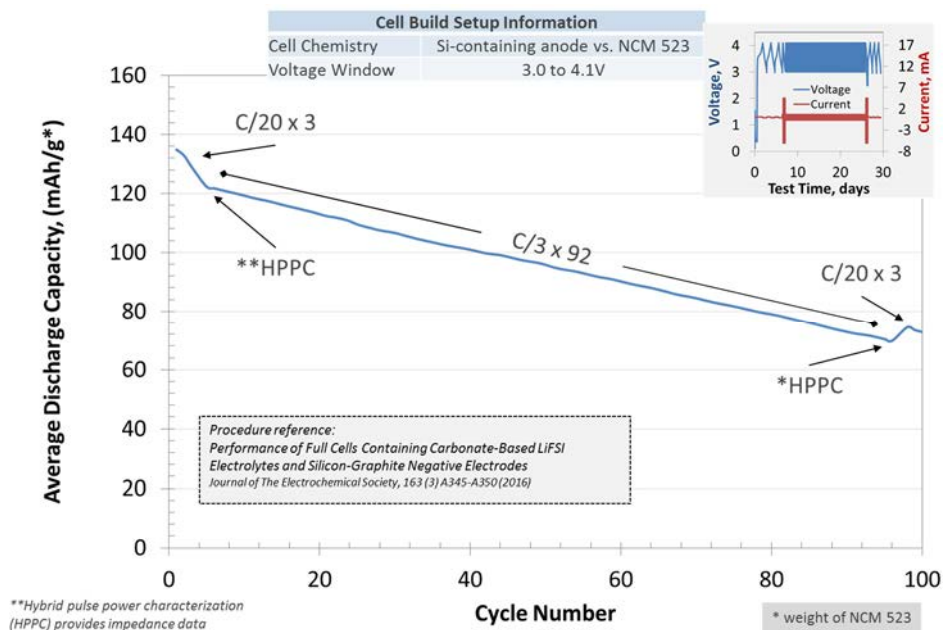


Figure 2. Full cell testing protocol.

As the program matures, materials developments will be incorporated into baseline silicon-based materials, electrodes, and cells. Scale-up of materials, incorporation of materials advancements into electrodes and prototype cells, and characterization and testing of cells, as well as evaluation of safety and abuse tolerance are part of a wide range of integrated studies supported by battery research facilities at the National Labs working closely with the program. These research facilities include the Battery Abuse Testing Laboratory (BATLab), the Battery Manufacturing Facility (BMF), the Cell Analysis, Modeling, and Prototyping (CAMP) facility, the Materials Engineering Research Facility (MERF), and the Post-Test Facility (PTF).

The fundamental understanding of silicon-based electrode active materials is based on extensive electrochemical and analytical diagnostic studies on components, electrodes, and cells conducted within the program. This effort contains in-situ and ex-situ studies on full and specialty cells, including reference electrode cells. Overall, the diagnostic studies are intended to help establish structure-composition-property relationships, including lithium-alloying surface and bulk transport and kinetic phenomena. Further, they should form the basis for accurately assessing component and electrode failure modes and lay a path for advancements.

Supported by the diagnostic studies, materials development on silicon-based materials, electrodes, and cells is being conducted to enhance interfacial stability, accommodate intermetallic volume changes, and improve overall performance and life. Key to this effort is the development and testing of coatings and additives designed to modify and stabilize the dynamic silicon-electrolyte interface. Further, functional polymer binders designed to accommodate volume changes, increase conductivity, and improve adherence are being developed and analyzed. Finally, the program is exploring active material development. Alternative high-energy silicon-alloy/composite materials are being considered. Also, strategies for introducing additional lithium inventory into the cell are being developed.

Communication of programmatic progress to battery community is critical. This will generally be accomplished through publications, presentations, reports, and reviews. Further, the program is open to industrial participation and/or collaboration that does not limit program innovation or the free flow of information. Finally, this program is highly integrated with our sister program on SEI-Stabilization, called SEI-Sta for short. In general, SEI-Sta is focused on the development and characterization of model systems, thin-film well-defined active area electrodes on which it is easier to extract fundamental information on lithium-silicon phase formation, lithium transport, and interfacial phenomena (e.g. SEI formation and growth).

References

1. *Alloy Negative Electrodes for Li-Ion Batteries*. M.N. Obrovac and V.L. Chevrier, Chem, Rev. 2014, 114, 11444-11503.
2. *Modeling the Performance and Cost of Lithium-Ion Batteries for Electric-Drive Vehicles*. Second Edition, Argonne National Laboratory Report, ANL-12/55.
3. *Performance of Full Cells Containing Carbonate-Based LiFSI Electrolytes and Silicon-Graphite Negative Electrodes*. S.E. Trask, K.Z. Pupek, J.A. Gilbert, M. Klett, B.J. Polzin, A.N. Jansen, and D.P. Abraham, Journal of The Electrochemical Society, 163 (3) A345-A350 (2016).

1. Research Facilities Support

CAMP Facility Support Activities

Steve Task, Alison Dunlop, Bryant Polzin, and Andrew Jansen (Argonne National Laboratory)

Background

The Cell Analysis, Modeling and Prototyping (CAMP) Facility at Argonne National Laboratory is providing support to this project in a number of different ways. The main contributions to the project are: providing standard materials, providing baseline electrodes (both anodes and cathodes) that are capacity matched, providing experimental electrodes as needed, and providing electrochemical data from coin cells and pouch cells that were tested by the CAMP Facility. By having access to these materials, (electrodes and data), other participating laboratories in the project are able to characterize and test the same materials using different techniques and are able to better compare data across all laboratories working in this project.

Results

In this quarter we decided to explore new high-silicon-content negative electrodes. The CAMP Facility's development of silicon-based electrodes began in 2012 with a focus on electrodes with ~70 % silicon and full utilization (lithiation to ~5 mV). These cells lost the majority of their capacity within 30 cycles. Limiting the lithiation to 1,000 mAh/g resulted in cycle life over 100 cycles, with low amounts (3 wt.%) of FEC in the electrolyte. While this was a significant improvement in cycle life, it was still far short of the 1,000 cycle goal. It was then decided to explore composite electrodes of silicon and graphite, where BatPac modeling indicated that an electrode with >30 wt.% Si, balanced with graphite, would result in an electrode with 1,000 mAh/cm³ (~1,300 mAh/g).

The CAMP Facility took the approach of starting with low additions of Si to a graphite composite electrode (using LiPAA binder) and incrementally increasing the Si to reach 30 wt.% Si. Good quality electrodes were made with 3 mAh/cm² for 5, 10, and 15 wt.% Si, but with correspondingly poorer cycle life with increasing amounts of Si (see previous AMR presentations). Since a cycle life of only ~80 cycles was achieved with 15 wt.% Si, it was decided that further increases in Si were not warranted. These efforts used high levels of lithiation with a lithiation cutoff voltage of 50 mV (vs. Li⁺/Li) to prevent the formation of the deleterious Li₁₅Si₄ phase. Overall, this approach of low silicon and high lithiation has not resulted in acceptable cycle life. A new approach is needed.

This year's effort is exploring the use of higher amounts of silicon (30-70%), but with lower levels of lithiation (~100 mV vs. Li⁺/Li). Using a lower level of lithiation will lessen the degree of silicon particle expansion, which should lessen the degree of damage to the silicon SEI film on repeated lithiation. However, a 100 mV lithiation cutoff potential will result in graphite not providing any significant capacity to the electrode because the lower voltage plateaus of graphite would not be utilized (see Figure 1). In fact, incorporating other conductive additives (*e.g.*, carbon black, hard carbon, carbon nanotubes, *etc.*) instead of graphite may be more effective in providing an electronic matrix. Not using graphite may also enable other binder systems to be employed. However, not utilizing the lower voltage plateaus of the graphite may lower the average cell voltage

by ~200 mV. This will hopefully be compensated for by an increased capacity density of the negative electrode.

Initial coating experiments were performed in this quarter using Si material from Paraclete Energy with a Si content near 71 wt.% and conductive carbon (C45) near 10 wt.%. These results are summarized in Figure 2, which depicts the results of the formation cycles versus lithium metal. In these cycles, the lithiation lower voltage cutoff was 50 mV so that a fuller picture of the voltage profile could be seen as a function of capacity. Using this lower cutoff most likely stressed the Si particle and caused an increase in the capacity fade rate. If the intended cutoff of 100 mV is used instead, it is estimated that 1,300 to 1,800 mAh/g of Si could be realized.

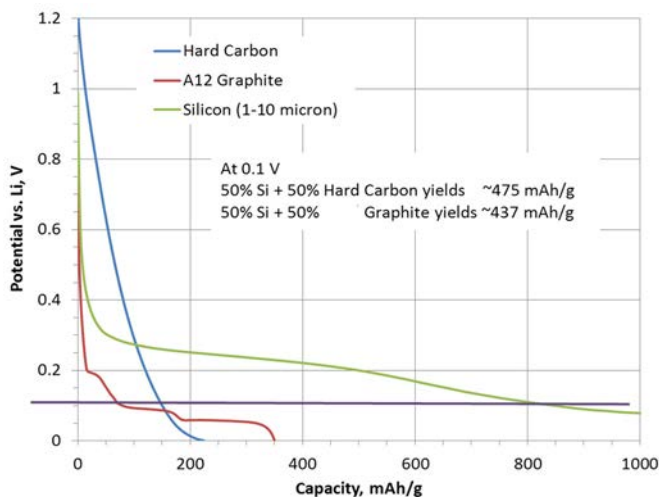


Figure 1. Lithiation voltage profiles of graphite, hard carbon, and silicon.

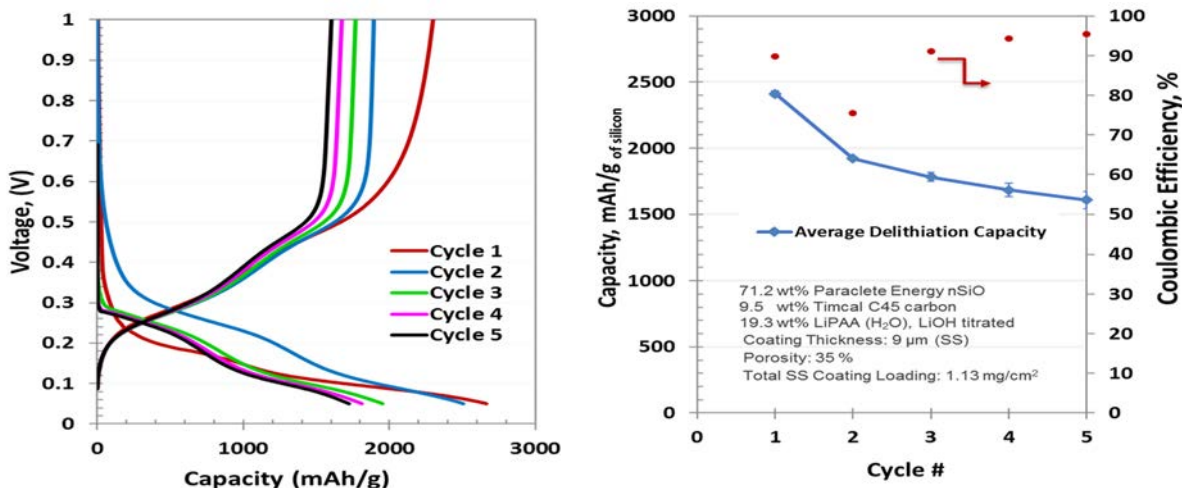


Figure 2. Initial electrochemical results of high silicon content (~70 wt.%) electrodes fabricated by CAMP Facility (at 50 mV cutoff) versus Li metal. No graphite was used in this electrode.

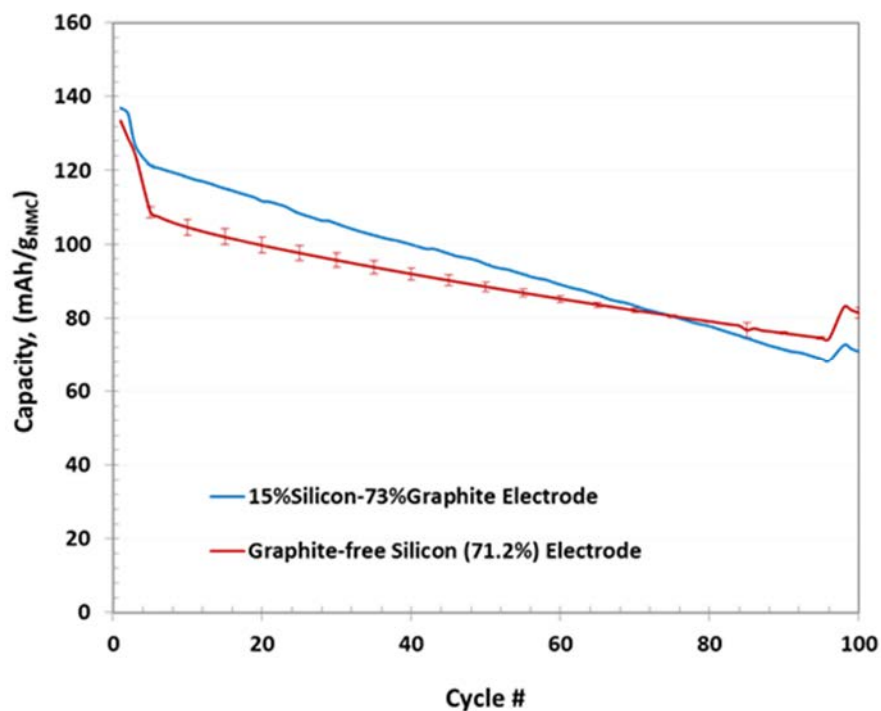


Figure 3. Comparison of the high-silicon (71 wt.%) anode to earlier 15 wt.% Si in graphite composite anode versus a common capacity-matched NMC532 cathode. A 50-mV lithiation cutoff was used for both anodes.

This high-silicon graphite-free anode was then tested in full-cell coin-cells with a capacity-matched NMC532 cathode. A 50-mV lithiation cutoff was used for this anode in the capacity matching so that a direct comparison could be made to the 15 wt.% silicon-in-graphite composite negative electrode developed earlier in this program, which is shown in Figure 3. While the initial capacity of the high-silicon cell is lower, its capacity fade rate is lower such that the high-silicon cell has higher capacity retention beyond the 70th cycle. A better cycle life is expected when the 100 mV lithiation cutoff is used in future experiments.

Conclusions

The inability to develop a silicon-graphite composite electrode that uses a low silicon content and a high degree of lithiation (50 mV vs. Li⁺/Li) with good cycle suggests that a new approach is needed. This quarter's effort was devoted to developing a high-silicon (71 wt.%) graphite-free anode with a plan to use lower levels of lithiation (100 mV vs. Li⁺/Li).

As in past quarters, the CAMP Facility continues to provide the materials and data necessary to the program so that the overall program can move forward with consistent results. The CAMP Facility will continue to provide material support to this program in future quarters and will present new data as it becomes available.

Surface Chemistry of the Oxide Shell and its Impact on Silicon-Based Battery Anodes

Kevin Hays, Beth Armstrong, and Gabriel Veith (Oak Ridge National Laboratory)

Background

Variation between various batches of silicon and silicon prepared by different methods makes it difficult to apply “successful” electrode fabrication techniques to all electrode systems. We believe by understanding the surface chemistry and how the surface chemistry changes between silicon electrode materials we can predictively direct the formation of suitable electrodes for long cycle life and long calendar life. In this work we investigated 4 different commercially viable electrode materials; two were prepared by milling and two were prepared by plasma deposition methods. We have found significant changes in the surface chemistries, even when nominally prepared by the same process.

Results

X-ray photoelectron spectroscopy (XPS) data collected for each powder, focused on the Si 2p region (Fig 1A), displays two unique features at binding energies of 99.4 eV and ~103-104 eV representing Si⁰ and SiO_x (1 ≤ x ≤ 2), respectively. The feature at 99.4 eV varies in intensity relative to the SiO_x feature, likely due to different SiO_x shell thicknesses. Furthermore, the SiO_x peak shifts from 102.6 to 103.8 eV. The shift in this peak increases with the oxidation state of the Si, as the surface approaches SiO₂. Based on these trends, milled P Si has the thinnest oxide shell while plasma AA Si has the thickest. Alternatively, the plasma HQ Si has the least O content within the SiO_x shell, while the plasma AA Si has the greatest O content.

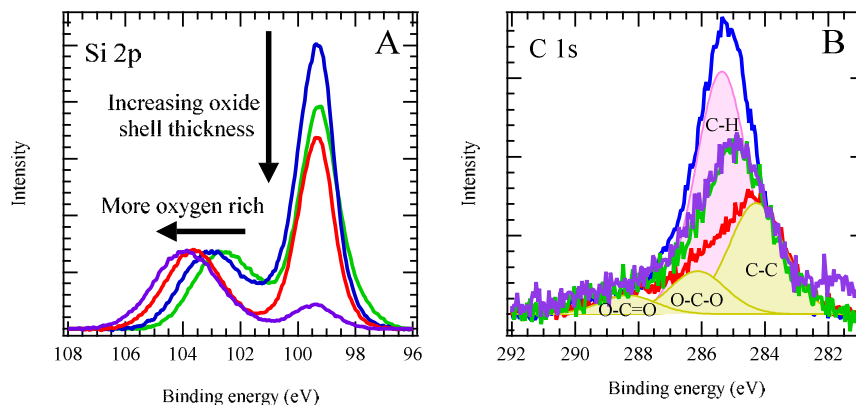


Fig. 1. XPS of four Si particles; Milled P (blue trace), Milled NA (red trace), Plasma HQ (green trace), Plasma AA (purple trace). A) Si 2p region, B) C 1s region, the yellow and pink filled regions are fitted from the milled P spectrum

Differences in the thickness of the oxide shell immediately stand out, but the role in minute changes to the surface chemistry are less obvious. Silica particles contain large amounts of silanol functionalities at the surface, which assist in charge stabilization of the particles in water, forming a stable colloid. [1] Similarly, Si particles with a SiO_x shell have previously been reported to share the same functionalities. [2] These silanol functionalities are not only important for dispersion but are also believed to be crucial in forming H-bonding networks with many successful binder systems for Si based anodes. [3] However, attenuated total reflectance – Fourier transform infrared spectroscopy (ATR-FTIR) of the commercial Si particles studied here indicate varying amounts of surface silanols (Fig. 2). Instead the surface functionalities are largely dictated by the synthesis method. In fact, even Si particles produced by a similar method (milled vs plasma synthesized) display unique surface features. All Si powders have some level of silanol functionality as indicated by the stretching vibration at 3750 cm⁻¹. Of the four, the plasma HQ Si has the strongest feature at this frequency.

Furthermore, it also has a broad band $800 - 950 \text{ cm}^{-1}$, also characteristic of Si-O-H stretching, not found with the other particles. [4] The broad band between $3200 - 3400 \text{ cm}^{-1}$ is often ascribed to H-bonded silanols, but more likely arises from residual water. Another prominent feature appears in the region of $2700 - 2950 \text{ cm}^{-1}$, due to CH_3 and CH_2 vibrations. [5] The milled P Si displayed the most significant amounts of these methyl groups, but the plasma synthesized particles indicate small amounts as well. This can further be confirmed by the C1s XPS spectra (Fig. 1B), which followed a similar trend with increasing amounts of C-H bonding at 285 eV, following the same trend as the ATR-FTIR spectra. The last important feature to note occurs at 2250 cm^{-1} in the ATR-FTIR spectrum of the plasma AA Si, resulting from Si-H vibrations. [5] There is evidence for this vibration in the other Si particles as well, but these features are not nearly as prominent. The plasma AA Si has an additional band at 850 cm^{-1} not present in other Si particles, representing O-Si-H bending, implying this Si-H bonding occurs at the surface SiO_x interface. Such bonding develops along with HF treatment of silica surfaces. [5]

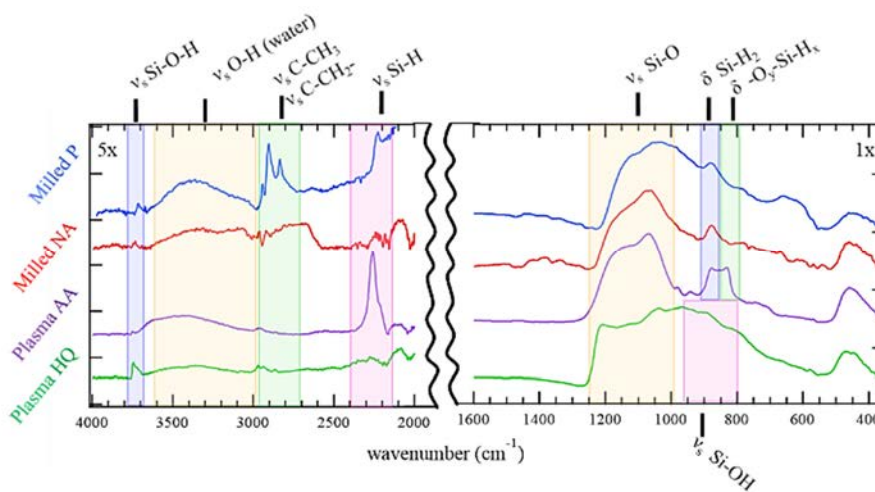


Fig. 2 ATR-FTIR of for commercial Si powders. Milled P (blue trace), Milled NA (red trace), Plasma HQ (green trace), Plasma AA (purple trace).

The differences in the surface chemistries are directly reflected in the electrochemical properties of these Si particles. The first cycle of Si- Li half cells utilizing each Si powder (Fig. 3) displays unique capacities and Coulombic efficiency values for each. Delithiation from 50 mV to 1.5 V, at 90 mA/g (~C/40), achieves a capacity of 2500 mAh g^{-1} for both milled particles. The plasma P Si was slightly less at 2230 mAh g^{-1} , while the plasma AA Si only obtained 1030 mAh g^{-1} . Coulombic efficiencies followed the oxide thickness trend demonstrated in figure 2A; milled P (81.4%) > plasma HQ (81.2%) > milled NA (76.3%) > plasma AA (57.7%). More surface area can lead to greater amount of electrolyte decomposition, [6] but both plasma synthesized Si particle have similar surface areas at $\sim 45 \text{ m}^2 \text{ g}^{-1}$, while the milled particles are less at $30 \text{ m}^2 \text{ g}^{-1}$ and $14 \text{ m}^2 \text{ g}^{-1}$, for the milled p and milled NA Si respectively. This lack of correlation in the surface area means electrolyte decomposition alone cannot be the sole reason for differences in first cycle Coulombic efficiencies.

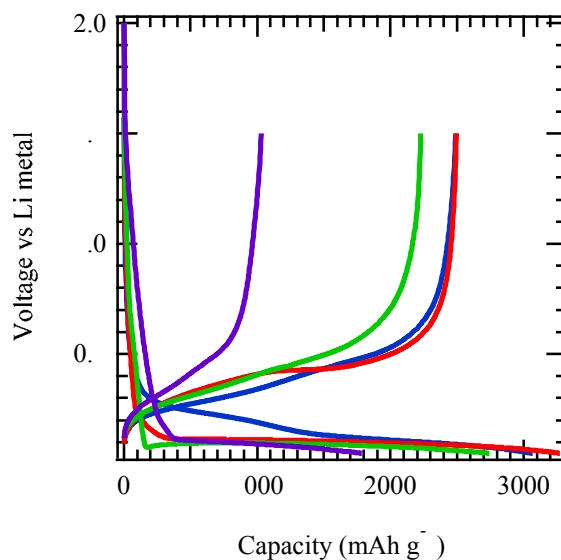


Fig. 3 First cycle voltage profiles of Si-Li half cells cycled at 90 mA g^{-1} from 0.05 to 1.5 V vs Li metal. Milled P (blue trace), Milled NA (red trace), Plasma HQ (green trace), Plasma AA (purple trace).

Conclusions

In summary, four commercial Si particles were investigated for Li-ion battery anodes. With max capacity of $\sim 2500 \text{ mAh g}^{-1}$, differences arise in the oxide layer of each particle. XPS matched electrochemical data insinuating varying thicknesses of oxide layers. ATR-FTIR saw changes in surface functionalities of each Si particle, indicating sparse presence of surface silanol functionalities. This impacts how aqueous based binders may interact with the Si particles or how the surface can be modified as many of reactions occur at the silanol functionalities.

References

1. Zhuravlev, L. T., The surface chemistry of amorphous silica. Zhuravlev model. *Colloid Surface A* **2000**, *173* (1-3), 1-38.
2. Xun, S.; Song, X.; Wang, L.; Grass, M. E.; Liu, Z.; Battaglia, V. S.; Liu, G., The Effects of Native Oxide Surface Layer on the Electrochemical Performance of Si Nanoparticle-Based Electrodes. *Journal of The Electrochemical Society* **2011**, *158* (12), A1260-A1266.
3. Hochgatterer, N. S.; Schweiger, M. R.; Koller, S.; Raimann, P. R.; Wöhrle, T.; Wurm, C.; Winter, M., Silicon/Graphite Composite Electrodes for High-Capacity Anodes: Influence of Binder Chemistry on Cycling Stability. *Electrochemical and Solid-State Letters* **2008**, *11* (5), A76-A80.
4. Smith, A. L., *Analysis of silicones*. Wiley: 1974.
5. Ubara, H.; Imura, T.; Hiraki, A., Formation of Si-H bonds on the surface of microcrystalline silicon covered with SiO_x by HF treatment. *Solid State Commun.* *50* (7), 673-675.
6. Winter, M.; Novak, P.; Monnier, A., Graphites for lithium-ion cells: The correlation of the first-cycle charge loss with the Brunauer-Emmett-Teller surface area. *J. Electrochem. Soc.* **1998**, *145* (2), 428-436.

Thermodynamic Understanding and Abuse Performance

Kyle Fenton, Eric Alcorn, and Ganesan Nagarajan (Sandia National Laboratories)

Background

As we develop new materials to increase performance of lithium ion batteries for electric vehicles, the impact of potential safety and reliability issues become increasingly important. In addition to electrochemical performance increases (capacity, energy, cycle life, etc.), there are a variety of materials advancements that can be made to improve lithium-ion battery safety. Issues including energetic thermal runaway, electrolyte decomposition and flammability, anode SEI stability, and cell-level abuse tolerance behavior. Introduction of a next generation materials, such as silicon based anode, requires a full understanding of the abuse response and degradation mechanisms for these anodes. This work aims to understand the breakdown of these materials during abuse conditions in order to develop an inherently safe power source for our next generation electric vehicles.

The effect of materials level changes (electrolytes, additives, silicon particle size, silicon loading, etc.) to cell level abuse response and runaway reactions will be determined using several techniques. Experimentation will start with base material evaluations in coin cells and overall runaway energy will be evaluated using techniques such as differential scanning calorimetry (DSC), thermogravimetric analysis (TGA), and accelerating rate calorimetry (ARC). The goal is to understand the effect of materials parameters on the runaway reactions, which can then be correlated to the response seen on larger cells (18650). Experiments conducted showed that there was significant response from these electrodes. Efforts to minimize risk during testing were taken by development of a smaller capacity cylindrical design in order to quantify materials decision and how they manifest during abuse response.

Results

This work continues the efforts from last year, which aim to understand the fundamental reactions and quantify response from silicon based anodes under abusive conditions. This included evaluation of anodes containing between 0 and 15 wt% silicon from a variety of sources. Investigations were completed on coin cell and 1.25 Ah 18650 form factors. Several experiments showed a high level of gas generation and overall runaway for cells containing silicon electrodes. To further understand the response of these materials, this work focused on understanding the effect of several factors impacting runaway response and gas generation including solvent selection, electrode processing, silicon content, and the effect of water. Previous efforts to evaluate these parameters in 18650 cell form factors using accelerating rate calorimetry (ARC) proved difficult due to the gas generation and temperatures involved during runaway. In order to try and quantify these effect, 18650 cells were made with electrodes cut to a much smaller overall cell capacity of roughly 600 mAh nominal capacity. Figure 1 shows the ARC response for 18650 cells with 15 wt% silicon. Results are shown for two different silicon ARC evaluations (green and yellow). This behavior shows the incredibly inconsistent responses observed using cells with silicon anodes. Heat generation, gas generation, and overall response is not easy to predict.

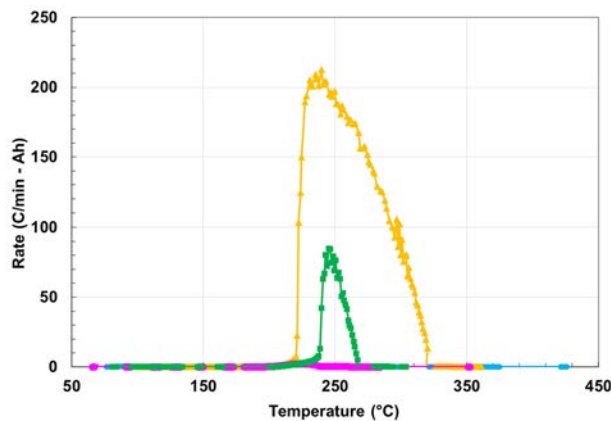


Figure 1 - Accelerating rate calorimetry (ARC) response for 18650 cells with 15 wt% silicon. Response is shown for two separate samples, shown in green and yellow. Heating rate is not normalized to active material content, so peak heating rates and overall runaway enthalpy is shown for qualitative purposes only.

Figure 2 shows a subset of data from the analysis done on gas samples that were taken during ARC testing. This was done to try and evaluate species evolved during runaway. Similar to previous reports, the baseline graphite cells (grey) show less short chain hydrocarbon generation. Silicon containing materials show increased ethane generated during runaway. This indicates a higher degree of reactivity for cells containing the silicon based anodes.

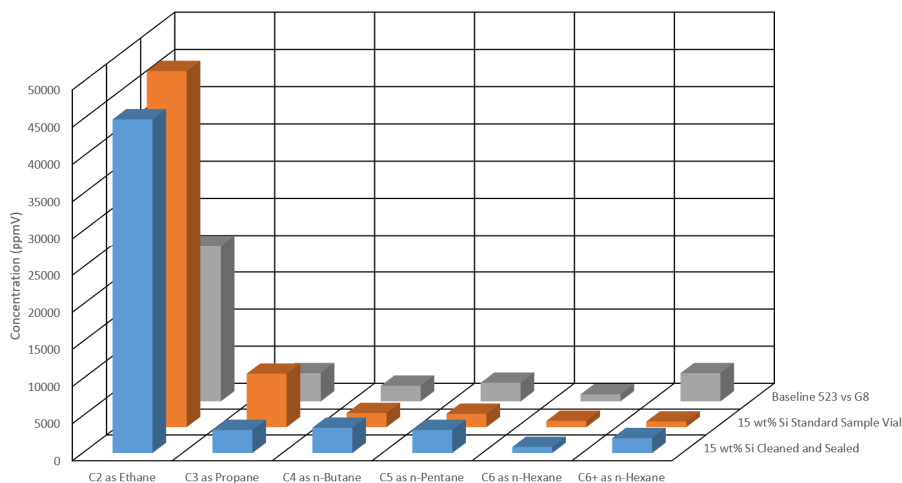


Figure 2 - Gas sampling data that compares hydrocarbon generation during runaway.

Conclusions

This work demonstrates that there is an impact on safety response with nanoscale silicon materials compared to graphite based anodes. Additionally, there appears to be a fundamental difference in abuse response based on more than just silicon content, particle size, and state of charge for the electrodes. Control of surface reactivity is essential to both control response homogeneity (for quantification) and understand the mechanisms during abuse conditions with silicon anodes.

Hydro/Solvothermal Synthesis and Scale-up of Silicon and Silicon-Containing Nanoparticles

Youngho Shin, Gregory K. Kumnick (Argonne National Laboratory)

Background

The immediate objective of this project is to develop and set up an advanced bench-scale hydro/solvothermal synthesis system for the production and evaluation of high-capacity engineered silicon nanoparticles and composites used as the active anode material in Li-ion batteries. These materials need to be tested and validated in large format prototype cells before going to high-volume manufacturing which use a fair amount of material. For this reason, the synthetic capability to be developed would be based on the design and construction of a turnkey hydro/solvothermal synthesis reactor system capable of batch production of 10 to 50 g of nanoparticles per run.

One of the features of the present process is to provide a bottom-up synthesis approach (stacking atoms onto each other) of silicon nanoparticles and composites which is more advantageous than the common top-down synthesis approach (etching out crystals planes) because the former has a better chance of producing nanostructures with less defects, more homogenous chemical composition, and better short- and long-range ordering. Using this advanced bottom-top synthesis approach, the crystallinity, particle shape and size of silicon nanoparticles incorporated into their composites, which are the key parameters of these materials' failure, should be intensely investigated and optimized to support the fundamental understanding of the EERE-VTO Energy Storage Si Deep Dive projects.

Results

Most methods of silicon-based anodes are those that produce SiO_x-based materials which include commercially available SiO_x powders either directly mixing with carbon (e.g., graphite) or surface carbon coating using organic sources. To conduct a systematic study on the synthesis of silicon-based anodes, we are building the ability to synthesize Si nanoparticles in various sizes and shapes. Based on this ability, it is possible to perform systematic synthesis to achieve optimal Si/C composite.

Anodes made from a Si/C composite can combine the favorable properties of carbon (long cycle life) and silicon (high lithium storage capacity) to improve the overall electrochemical performance of the anode of a lithium ion battery. The need for synthetic studies such as Si/C composites is due to providing a means to mitigate mechanical stress changes induced by the large volumetric change should be buffered to achieve better cycle performance of silicon-based anodes. For this purpose, the size and morphology control of silicon nanoparticles is critical to inhibiting mechanical failure in the silicon-based anode cycle. In addition, the sphericalization of Si/C composite is required. This is because the spherical particles induce an improved tap density, so that the resulting spherical composite is highly desirable as an anode material for a lithium-ion battery.

We can produce hydrophilic carbon materials in the form of spheres at 300 °C or higher as well as water-soluble carbohydrates heated to about 200 °C by using the currently installed hydro/solvo thermal reactor. A simplified reaction mechanism for the formation of the carbon spheres involves the dehydration of the carbohydrate in the first step and subsequent polymerization and carbonization of the thus generated organic compounds in the second step. The resulting droplets form either the final spherical carbon particles or they can be used for nano-coating other structures.

On the basis of production cost and promotion, our interest in the development of Si/C composite materials is to find a simple synthesis pathway to produce Si/C composites with nanoscale Si particles uniformly distributed. To achieve this goal, we will use both Si nanoparticle synthesis route starting from Si chemical (ex. TEOS) and commercially available Si nanoparticle application route. We plan to conduct preliminary synthesis and evaluation of Si/C composite containing 0%, 10%, 20% and 30% silicon. Then we will proceed

with the pouch cell evaluation in CAMP by determining the desired synthetic pathway and carrying out a material scale-up to 100 grams each. Based on the analysis of the synthesized materials and the feedback of the pouch cell evaluation, we will gradually produce an improved type of silicon-based anode materials.

Si/C Composite Synthesis Strategy

	<input type="checkbox"/> Embed Si using Si Chemicals	<input type="checkbox"/> Embed Si using Si Nano-particles
Predicted Features	<ul style="list-style-type: none"> ▪ Si shape control: rod or sphere ▪ Si size control: 10 ~ 200 nm ▪ No Si aggregation (uniform distribution) ▪ Improvement to graphite-free Si-metal composite 	<ul style="list-style-type: none"> ▪ Limit to particle shape used ▪ Limit to particle size used ▪ Si aggregation from raw material ▪ Lower manufacturing cost
Preliminary Synthesis & Coin half cell	Fixed Si shape and size using same rxn condition 0% Si/C, 10% Si/C, 20% Si/C and 30% Si/C Optimize post heat treatment	Selection of a commercial Si Nano-particle 0% Si/C, 10% Si/C, 20% Si/C and 30% Si/C Optimize post heat treatment
GO/NO-GO	Synthesis route will be selected based on coin half cell evaluation	
100 gram Scale-up	0% Si/C, 10% Si/C, 20% Si/C and 30% Si/C	
Pouch cell test @CAMP	Best Si content will be determined based on pouch cell evaluation	
Advanced Characterization	Check mechanical failure and side reaction by collaborators	
1st Round End GO/NO-GO New Round Start	Feed back from CAMP & collaborators Kilogram production and/or new material synthesis approach <ul style="list-style-type: none"> ▪ Optimize the size of Si nanoparticles to mitigate mechanical failure ▪ Investigate the shape effect of Si nanoparticles ▪ Evaluate composite materials such as graphite, graphene, and CNT ▪ Investigate graphite-free Si-metal composite 	

Figure 1. Strategy of Si/C composite synthesis, scale-up, pouch cell evaluation, and further improvement

Conclusions

4L hydro/solvo thermal system is under construction and safety planning with the aim of operation permission in August and commissioning in September. After that, Si/C composites will be synthesized from two raw materials, Si chemical and Si nanoparticle. Si/C composite materials scaled will undergo pouch cell evaluation in CAMP.

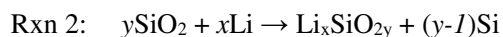
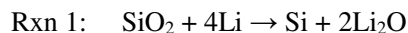
2. Characterization, Dagnostics, and Analysis

Lithium Silicate Formation Investigated by FTIR

Rose E Ruther, Kevin A. Hays, Gabriel M Veith, and Jagjit Nanda (Oak Ridge National Laboratory)
Jaclyn Coyle (Sandia National Laboratory) Boris Key (Argonne National Laboratory)

Background

An oxide layer is present on the surface of any silicon exposed to air. The fate of this oxide during electrochemical lithiation of silicon-based anodes is still unclear. Two reactions that have been proposed in the literature are: [1-3]



We showed that Rxn 2, which forms lithium silicates, could be followed using FTIR spectroscopy. [4] However, these experiments were performed using silicon-graphite composite electrodes with only 15 wt.% silicon. To better isolate the signals from the silicon oxide, nanoparticle silicon electrodes without graphite were fabricated with a minimal amount of conductive carbon black and LiPAA binder. A large-format, single-layer pouch cell was constructed to produce enough material for complimentary characterization by NMR at ANL. The electrode was harvested after one cycle of lithiation/delithiation. Complete characterization of the oxide interface is important since it influences electrolyte decomposition, lithiation kinetics, and binder interactions.

Results

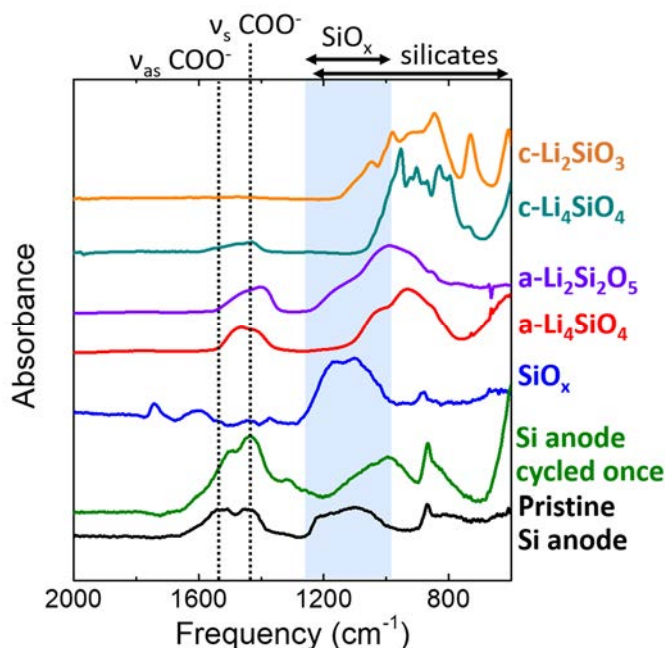


Figure 1. FTIR spectra of a pristine Si anode, cycled Si anode, and reference compounds. The silicon oxide band in the pristine anode shifts to lower frequency after one electrochemical cycle consistent with partial lithiation of the oxide to form lithium silicates.

Silicon oxide has a broad band from $\sim 1000 - 1250 \text{ cm}^{-1}$ in the FTIR spectrum (Figure 1). After one electrochemical cycle this band clearly shifts to lower frequencies and partially overlaps the expected bands for lithium silicates. For comparison, reference FTIR spectra were acquired for crystalline and amorphous lithium

silicates. Crystalline lithium silicates were synthesized using solid state reaction, and amorphous silicates were deposited using RF magnetron sputtering. [5] The silicate band from the cycled anode is a good match for an amorphous silicate with relatively low lithium content.

The FTIR results agree with the calculated phase diagram (K. Persson, LBNL), which predicts that SiO_2 will lithiate and form increasing Li-O and Li-Si bonds, at the expense of Si-O. However, NMR analysis of the same cycled electrode shows that most of the silicon oxide remains a- SiO_x after cycling. Combining the results from FTIR and NMR may indicate that the actual composition of the surface layer is closer to a- SiO_x with small amounts of dissolved lithium.

Conclusions

From FTIR analysis, the surface oxide on silicon appears to lithiate during the first electrochemical cycle to form lithium silicates. Comparison with reference spectra indicates the silicate is relatively lithium poor. In contrast NMR does not support significant conversion of SiO_x to lithium silicates. Rather, NMR shows that the contribution from the a- SiO_x phase remains largely unchanged after cycling. The actual stoichiometry of the surface layer may therefore be closer to a- SiO_x with small amounts of dissolved lithium.

References

1. Philippe, B.; Dedryvere, R.; Allouche, J.; Lindgren, F.; Gorgoi, M.; Rensmo, H.; Gonbeau, D.; Edstrom, K., Nanosilicon Electrodes for Lithium-Ion Batteries: Interfacial Mechanisms Studied by Hard and Soft X-Ray Photoelectron Spectroscopy. *Chem. Mat.* 2012, 24, 1107-1115.
2. Guo, B. K.; Shu, J.; Wang, Z. X.; Yang, H.; Shi, L. H.; Liu, Y. N.; Chen, L. Q., Electrochemical Reduction of Nano- SiO_2 in Hard Carbon as Anode Material for Lithium Ion Batteries. *Electrochem. Commun.* 2008, 10, 1876-1878.
3. Kim, T.; Park, S.; Oh, S. M., Solid-State NMR and Electrochemical Dilatometry Study on Li^+ Uptake/Extraction Mechanism in SiO Electrode. *J. Electrochem. Soc.* 2007, 154, A1112-A1117.
4. Ruther, R. E.; Hays, K. A.; An, S. J.; Li, J.; Wood, D. L.; Nanda, J., Chemical Evolution in Silicon-Graphite Composite Anodes Investigated by Vibrational Spectroscopy. *ACS Appl. Mater. Interfaces* 2018, 10 (22), 18641-18649.
5. Coyle, J.; Apblett, C.; Brumbach, M.; Ohlhausen, J.; Stoldt, C., Structural and Compositional Characterization of RF Magnetron Cosputtered Lithium Silicate Films: From $\text{Li}_2\text{Si}_2\text{O}_5$ to Lithium-Rich Li_8SiO_6 . *J. Vac. Sci. Technol. A* 2017, 35 (6), 061509.

Inherent Reactivity Studies of Lithium Silicides

Baris Key, Binhong Han, Fulya Dogan, Jack Vaughey (Argonne National Laboratory)

Background

One of the core problems associated with Li-Si chemistry in Li-ion batteries is the inherent reactivity of the lithium silicides, the active material that forms upon the lithiation. These phases can react with almost all battery components such as binders, electrolytes, additives and impurities such as moisture and air which cause major coulombic losses and loss of lithium.

Results

A synthetic and characterization effort was undertaken to prepare key model compounds in the Li-Si phase diagram. In previous reports, X-ray diffraction and Solid State Magic Angle Spinning (MAS) NMR spectroscopy have been used to qualitatively and quantitatively study the potential reactions between the lithium silicides model compounds and different binder materials, such as LiPAA and PVDF. It is found that compared with PVDF, LiPAA lead to less chemical shifts in ^7Li and ^{29}Si MAS NMR results after mixed and ground with Li_7Si_3 model compounds (previously reported in quarterly reports), which according to the

previous NMR study [1, 2] representing less delithiation of lithium silicides and better chemical stability in contact with the charged Si species. However, the real degradation mechanism of PVDF is still unknown, which is critical to understand the origin of binder instability and improve the lifetime of Si anodes in the future.

To explore the degradation mechanism of PVDF in contact with the lithium silicides, the ^1H , ^{13}C and ^{19}F MAS NMR spectra of the mixture of Li_7Si_3 and PVDF were measured, as shown in Figure 1. Compared with the pristine PVDF, the mixture of Li_7Si_3 and PVDF showed a broadened ^1H peak and several new and broad aliphatic ^{13}C peaks, indicating the potential breakage of C-H and/or C-C bonds in the PVDF ($-\text{CH}_2-\text{CF}_2-$)_n structure. In the case of ^{19}F NMR results, although the relative peak intensities changed after mixing PVDF with Li_7Si_3 , no obvious peak broadening or new chemical environments, including LiF, was observed, indicating that the C-F bonds are relatively stable during the degradation of PVDF in contact with Li_7Si_3 . Therefore, the intensity changes for the C-F sites are mainly correlated to the changes in the adjacent C-C and C-H bonds.

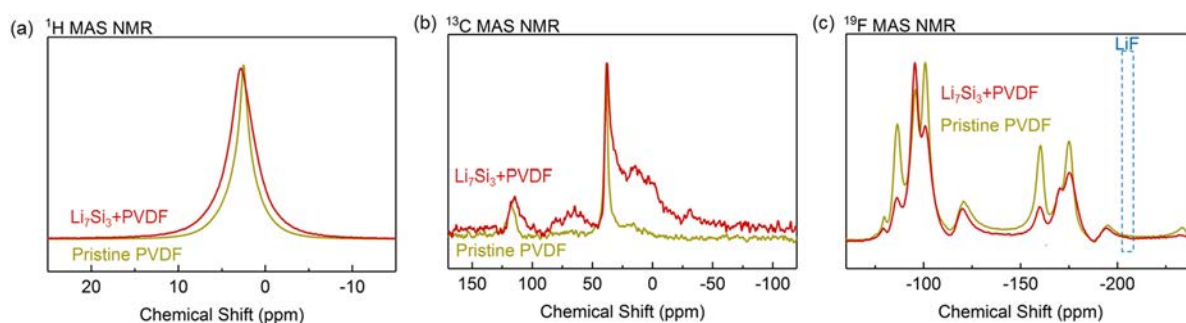


Figure 1. (a) ^1H , (b) ^{13}C , and (c) ^{19}F MAS NMR spectra of pristine LS samples and their mixture with 10 wt% PVDF..

Since the potential cleavage of C-H bonds by Li_7Si_3 may lead to the formation of H_2 , here to confirm the real PVDF degradation mechanism, we designed a special gas-trapping setup to determine a gas generation (presumably H_2 , the only chemically relevant alternative) after mixing PVDF with Li_7Si_3 . Initially, pristine PVDF powder and pristine ground LS powder were put at the two ends of a glass vial, as shown in the top left image in Figure 2, to minimize their contact before mixing. A hole was drilled on the cap of the vial, and a flat balloon was attached to the cap to catch any generated gas. The airtight cap with additional parafilm sealing ensured gas leakage. Then the sealed system was hand-shaken for 10 min to physically mix the PVDF with Li_7Si_3 . Due to the loose contact and limited mixing between LS and PVDF after the hand shaking, no immediate gas generation was observed after the mixing, as shown in the bottom left image in Figure 2. After sitting in the glovebox for 1 day, notable gas formation was observed with the balloon being inflated, as shown in the right image in Figure 2.

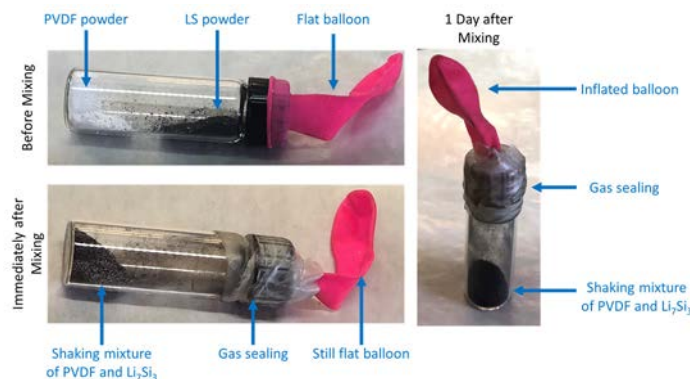
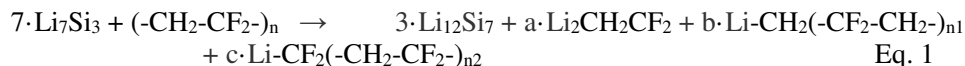
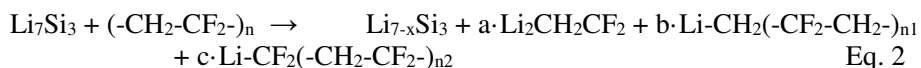


Figure 2. Images of gas-cathcing setup before, immediately after, and 1 day after the mixing of PVDF and Li_7Si_3 .

Based on the above results, here we propose several potential reactions between Li_7Si_3 and PVDF after physical mixing. In one possibility, the severe delithiation of Li_7Si_3 in contact with PVDF may formation of lower-Li-concentration phases such as $\text{Li}_{12}\text{Si}_7$. Meanwhile, the C-C bonds may be broken and lithiated to form organolithium complexes. The reaction could be written as below:



Here $a + b + c = 13$, representing different amounts of Li complexes formed. Since the phase transition from Li_7Si_3 to $\text{Li}_{12}\text{Si}_7$ requires major changes in the Si-Si connectivity, such reaction maybe kinetically hindered. In another possibility, Li may leave the Li_7Si_3 structure, forming a lower lithium content silicide phase with crystalline, semi-crystalline, or even amorphous structures. This will give us:

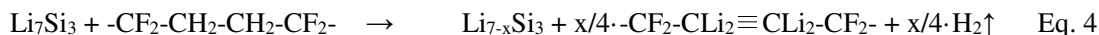


Here $a + b + c = x$.

In addition to the C-C bonds, the C-H bonds could also be broken and lithiated after mixing Li_7Si_3 with PVDF, while protons being reduced to H_2 , as shown in Figure 2. The reaction can be written as below:



Moreover, in PVDF there are usually structural defects, such as the existence of $-\text{CF}_2-\text{CH}_2-\text{CH}_2-\text{CF}_2-$ sequencing. [3, 4] The replacement of two adjacent C-H bonds with C-Li bonds may overly reduce the C-C bond to a $\text{C} \equiv \text{C}$ triple bond, as is shown below:



In all reaction equations listed above, the C-F bonds were keep intact, since no PVDF deflourization or LiF formation was observed in ^{19}F NMR after the reaction between Li_7Si_3 and PVDF.

Conclusions

NMR results showed that the C-F bonds in PVDF are relatively stable when mixing and grinding it with the Li_7Si_3 . On the contrary, C-H and C-C bonds in PVDF can be broken by the reducing lithium silicides, formation H_2 gas and lithium complexes, which could explain degradation and failure of Si anodes in electrochemical tests. Several viable chemical reactions between PVDF and Li_7Si_3 were proposed. The data and observations support these major side reactions detrimental to the electrochemistry and safety.

References

1. B. Key, R. Bhattacharyya, M. Morcrette, V. Seznec, J-M. Tarascon, C. P. Grey, J. Am. Chem. Soc., 2009, 131 (26), pp 9239–9249
2. B. Key, M. Morcrette, J-M. Tarascon, C. P. Grey, J. Am. Chem. Soc., 2011, 133 (3), pp 503–512
3. Russo, S.; Behari, K.; Chengji, S.; Pianca, M.; Barchiesi, E.; Moggi, G., Synthesis and microstructural characterization of low-molar-mass poly(vinylidene fluoride). Polymer 1993, 34 (22), 4777-4781.
4. Holstein, P.; Harris, R. K.; Say, B. J., Solid-state ^{19}F NMR investigation of poly(vinylidene fluoride) with high-power proton decoupling. Solid State Nuclear Magnetic Resonance 1997, 8 (4), 201-206.

Effect of High-Energy Ball Milling on the Electrochemical Performance of Silicate-Coated Silicon Nanoparticles

Linghong Zhang, Kaushik Kalaga, Wenquan Lu (Argonne National Laboratory)

Background

A Li_2SiO_3 coating has been reported beneficial for Li-ion batteries. When such a coating is present for a $\text{LiNi}_{0.6}\text{Co}_{0.2}\text{Mn}_{0.2}\text{O}_2$ cathode, improvement in both rate and cycle performance is observed owing to the excellent ionic conductivity of Li_2SiO_3 as well as the enhanced structural stability it provides[1]. A coating containing Li_2SiO_3 has also been applied to the Si anode. The resulting material showed improved capacity retention, however, with a compromised specific capacity.[2] Nonetheless, the improved capacity retention suggests that the Li_2SiO_3 coating may improve the mechanical stability of the Si nanoparticles. We have shown previously that we can successfully obtain silicate-coated Si nanoparticles through a solid-state reaction. The silicate layer consisted of a major component of Li_2SiO_3 with a fraction of Li_4SiO_4 . However, the particles were severely agglomerated after the solid-state reaction, and the capacity obtained from the electrochemical testing was low. In this report, we investigated the effect of high-energy ball milling using a Retsch Mill at breaking up the aggregates and its effect on the electrochemical performance of the silicate-coated Si nanoparticles.

Results

Figure 1 shows the diagram for the synthesis of silicate-coated silicon nanoparticles. To obtain the silicate-coated silicon nanoparticles with different silicate layer thicknesses, the Si nanoparticles with an average diameter of 80 nm were first treated at 400-600°C in the air for 15 hours to obtain a surface oxide layer of different thicknesses. The heat-treated Si nanoparticles were then mixed with Li_2CO_3 with a molar ratio of $n(\text{Si in SiO}_2) : n(\text{Li in Li}_2\text{CO}_3) = 1:4$, and heat-treated at 800°C under Ar atmosphere for 6 hours before collection for characterization.



Figure 1. Diagram for the synthesis of Li_2SiO_3 -coated silicon nanoparticles

The silicate-coated silicon sample was then characterized by scanning electron microscopy (SEM). Figure 2a shows that large agglomerates of 50-100 μm were present after the solid-state reaction between the silicon nanoparticles and the Li_2CO_3 . The presence of such agglomerates in the electrodes may result in difficulty of accessing the active silicon material inside the agglomerates, leading to low capacity in the electrochemical testing. We then investigated the effect of high-energy ball milling at breaking up the aggregates with help from the CAMP Facility at ANL. The silicate-coated silicon sample was first milled in an air-filled zirconia container containing 20 zirconia balls (2mm in diameter) for 5 minutes at 500 rpm using a Retsch Mill, and then milled in water for another 20 minutes. The resulting milled silicate-coated silicon sample was then collected and characterized under SEM. Figure 2b shows the SEM image of the ball milled silicate-coated silicon. Unlike the silicate-coated silicon after the solid-state reaction, the ball milled silicate-coated silicon showed no major agglomerates. The dynamic light scattering also confirmed the absence of larger agglomerates, further supporting the effectiveness of high-energy ball milling at breaking up agglomerates.

To test the effect of high-energy ball milling on the electrochemical performance of silicate-coated silicon, silicate-coated silicon samples of two different silicate thicknesses were synthesized. The silicate-coated silicon with a thinner silicate layer was obtained from the reaction between Li_2CO_3 and Si nanoparticles with

an oxide layer of 2.2 nm. The silicate-coated silicon with a thicker silicate layer was obtained from the reaction between Li_2CO_3 and Si nanoparticles with an oxide layer of 5.8 nm.

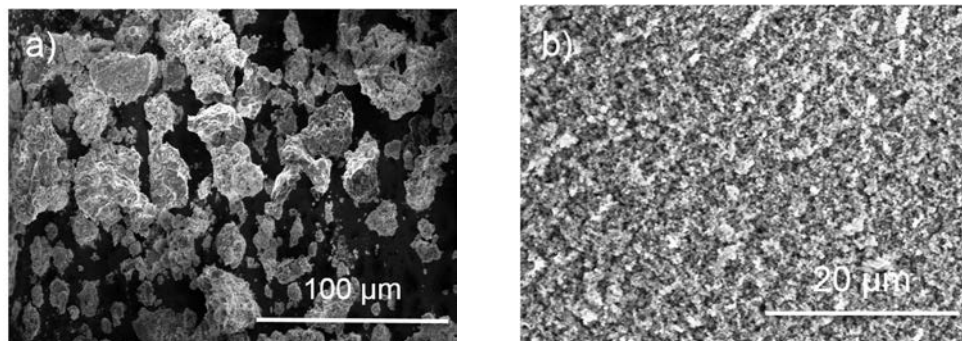


Figure 2 SEM of silicate-coated Si with starting Si nanoparticles of different oxide layer thicknesses

To fabricate the laminates for electrochemical testing, the silicate-coated Si samples were ball-milled with 20 wt% LiPAA and 10 wt% C45 using the Retsch Mill. The laminates were coated after different milling times. The electrodes were then punched from the laminates and tested in the half-cell configuration with Gen II electrolyte (EC: EMC=3:7, 1.2 M LiPF_6) with 10 wt% FEC. For formation test, the cells underwent three cycles at C/10 rate between 1.5 V and 0.01 V. Figure 3 compares the electrochemical performance of the electrodes made using the regular Thinky Mixer and the electrodes made using the Retsch Mill. Both silicate-coated silicon with a thinner silicate layer (shown in Figure 3a) and the silicate-coated silicon with a thicker silicate layer (shown in Figure 3b) showed worsened performance with high-energy ball milling process. The worsened performance suggest that the agglomeration may not be the key factor that leads to the poor electrochemical performance of the silicate-coated silicon.

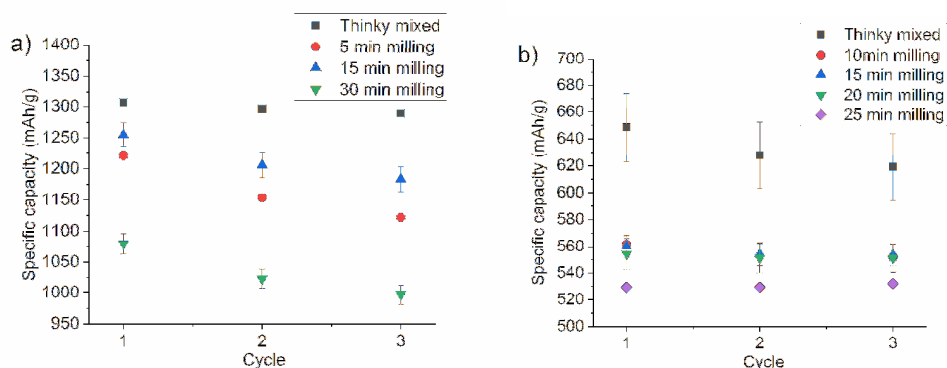


Figure 3 Electrochemical performance of formation cycles for high-energy-ball-milled silicate-coated Si with 3a) a thinner silicate layer and 3b) a thicker silicate layer.

Conclusions

High-energy ball milling using Retsch Mill was investigated on its effect on the electrochemical performance of silicate-coated silicon. Despite the fact that it is very effective at breaking up the agglomerates, the electrochemical performance of electrodes from ball-milling process was worse than the regular laminate fabrication using a Thinky Mixer. The result suggest that agglomeration may not be the key factor that leads to the poor performance. Better synthesis method to form silicate-coated silicon should be explored.

References

1. Wang *et al.* "Enhanced the electrochemical performance of lithium metasilicate-coated LiNiCoMnO_2 Ni-rich cathode for Li-ion batteries at high cutoff voltage", *Electrochimica Acta*, 2016, **222**, 806-819

- Lee *et al.* “High-performance silicon-based multicomponent battery anodes produced via synergistic coupling of multifunctional coating layers,” *Energy Environ. Sci.*, 2015, **8**, 2075-2084

Operando Quantification of Lithiation-Delithiation Behavior of Silicon-Graphite Composite Electrodes for Lithium-Ion Batteries

K.P.C. Yao, K Kalaga, J.S. Okasinski, JD. Amer, D.P. Abraham (Argonne National Laboratory)

Background

The use of blended silicon-graphite (Si-Gr) negative electrodes increases the energy density of lithium-ion cells over those containing only graphite (Gr) electrodes. However, the potentials and kinetics of lithium insertion into (and extraction from) Si and Gr are known to be different. Silicon is active in the entire 1.0 - 0.0 V range, whereas Gr is active only at potentials < 0.25 V vs. Li/Li⁺ during electrochemical cycling in (half) cells containing a Li-metal counter electrode. However, the relative lithiation/delithiation behavior of the Si and Gr components in blended electrodes is not well understood. Knowledge of the distribution of Li⁺ ions in the Si and Gr components is important because (in addition to electrode porosity) it determines the volume expansion of the blended electrode during electrochemical cycling. One reason for the knowledge gap is the amorphization of crystalline Si that occurs during lithium insertion, which makes it difficult to track the evolution of the component by techniques such as X-ray diffraction.

In this study, we conducted operando energy dispersive X-ray diffraction (EDXRD) to quantify lithiation/delithiation of Gr in a 15 wt% Si-Gr (Si-Gr) blended electrode; then, by taking into account the measured coulometric capacity of the cell we inferred the lithiation/delithiation behavior (and hence the volume changes) of the Si component. In parallel, we also conducted operando studies on a Gr electrode and used the data to calibrate behavior of the Gr component in the blended electrode. The EDXRD data were obtained at the 6BM-A beamline of Argonne’s Advanced Photon Source (APS). The 2032-type coin cell was used without any modification as the white beam (5 - 250 keV) penetrates the stainless steel casing.

Results

The electrode potential vs. capacity profiles and the XRD data from the operando lithiation and delithiation cycles are displayed in Figure 1. Prior to collecting these data, the 2032-type coin cells were cycled two times at a $\sim C/20$ rate in the 1.50 - 0.01 V vs. Li/Li⁺ (abbreviated as V_{Li}) range to form the SEI on the Gr (or Si-Gr).

The electrochemistry data in Figure 1 shows several plateaus in the voltage profile. On lithiation at $\sim C/30$ rate (Fig. 1a), starting from ~ 1.5 V to a 10 mV cut-off, three major plateaus are seen for the Gr-only electrode, at 0.202 (G1), 0.106 (G2), 0.072 V_{Li} (G3). For the Si-Gr electrode, five plateaus are observable at voltages values of 0.206 (G1), 0.116 (G2), 0.094 (S1), 0.078 (G3), 0.047 V_{Li} (S2). The delithiation (Fig. 1b) profile shows three plateaus for the Gr-only electrode at 0.111 (G4), 0.150 (G5), and 0.232 (G6) V_{Li} . These same three plateaus are also seen in the Si/Gr electrode data. In addition, the plateau at 0.429 V_{Li} (S3) is seen only in the Si/Gr electrode data. Plateaus S2 and S3 have been attributed to the crystallization of amorphous Li_xSi_y to $Li_{15}Si_4$ below ~ 50 mV during lithiation and its subsequent delithiation above ~ 400 mV, respectively. The plateau S1 likely arises from structural changes in the (amorphous) Si component that continue during the change in graphite potential from the plateau G2 to G3.

XRD data collected during the electrochemical cycling are presented in Figure 1c and 1d. Given that the strongest diffraction peaks belonging to the (00l) family of planes of the Li-Gr intercalation system occur within the range 3.2-3.8 Å, only this region is presented. It is worth noting that no spectral peaks were observed that could be attributed to a crystalline phase of Si; this observation is in agreement with prior research, which indicates that the crystalline Si becomes X-ray amorphous after the initial lithiation.

A custom computer code was written to deconvolute the Li_xC_y phases observed in the XRD patterns. After this deconvolution, the average Li^+ content (i.e., capacity) of the Gr component was quantified from the XRD peak intensities. For the Si-Gr electrode, the lithium content of the Si-component was obtained by subtracting the Gr capacity from the total cell capacity: the results are as portrayed in Figure 2.

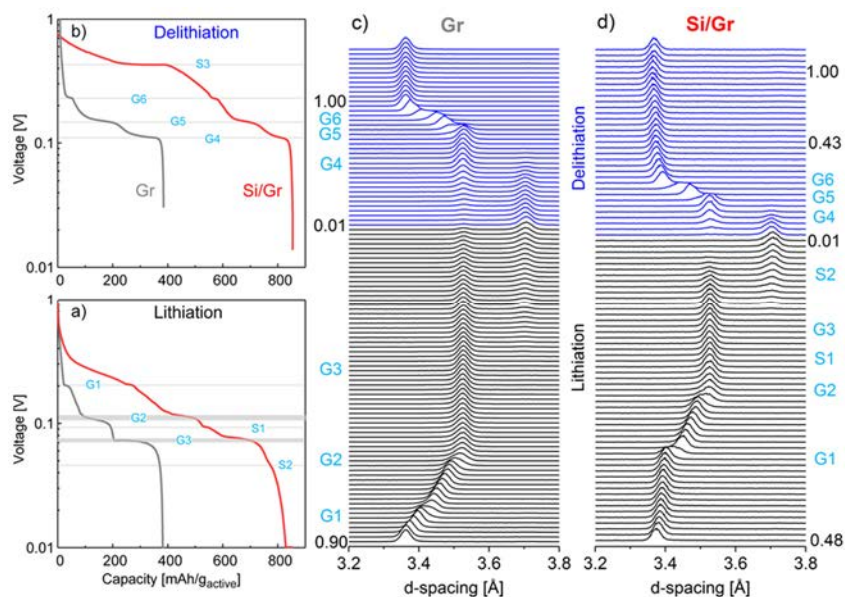


Figure 1. Electrode potential vs. capacity during lithiation (a) and delithiation (b) of a Gr-only electrode (grey line) and of a Si/Gr (15/73 w/w, red line) blended electrode cycled vs. Li metal. Operando XRD spectra (shown in the 3.2 to 3.8 Å d-spacing range) collected during the electrochemical cycling in (a) and (b) for the Gr-only (c) and Si-Gr (d) electrodes. Spectra collected on lithiation and delithiation are shown in black and blue coloring, respectively.

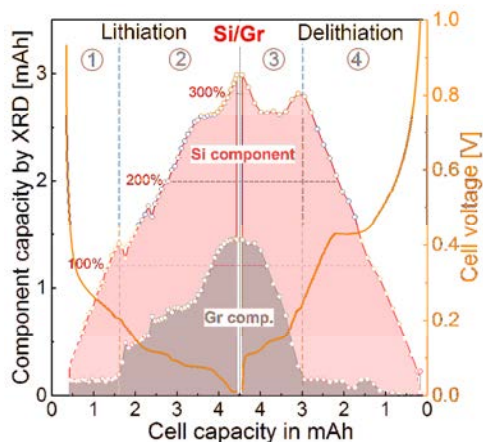


Figure 2. Capacity of the Gr and Si components of a Si/Gr (15/73 w/w) composite electrode during lithiation and delithiation (see cell voltage overlay, right y-axis). The x-axis shows the capacity measured using theycler. The capacity of the graphite component and silicon component are shown on the left y-axis. The percentages shown on the plot indicate volume expansion of the Si component during electrochemical cycling. Four distinct regions (discussed below) are indicated in the plot.

Conclusions

Operando energy dispersive XRD was conducted on 2032-type coin cells to monitor the evolution of the Gr-component in a composite Si/Gr (15/73, w/w) electrode during lithiation/delithiation cycling. Deconvolution of the Gr peaks combined with quantitative XRD analysis allowed us to monitor of the (de)lithiation fraction in each active component. The lithiation begins with Li^+ ion storage mainly in Si (region 1 in Figure 2); the Gr intercalates Li^+ ions only at potentials <0.20 V. In the $0.20 - 0.01$ V range, the relative lithiation of Si and Gr

are ~58% and 42%, respectively (region 2 in Figure 2). On delithiation, Li^+ extraction occurs mainly from Gr in the 0.01 – 0.23 V range (region 3) and from Si in the > 0.23 – 1.50 V range (region 4 in Figure 2); that is, the delithiation current is carried sequentially, first by graphite and then by silicon. This type of information can be used for the rational selection of electrochemical cycling windows that limits volumetric expansion in Si particles and thereby extending cell life.

3. Materials Advancements

Critical Role of Supporting Materials for Silicon Lithium-Ion Batteries

Bin Hu, Ssi Jang, Zengcheng Zhang, and Lu Zhang (Argonne National Laboratory)

Background

In this project, we have been working on understanding and re-engineering the crucial supporting materials for silicon lithium-ion batteries. Some efforts include understanding the property/cycling relationship of PAA binders, and re-engineering PAA based binders. [1] In this quarter, several items will be discussed: Firstly, as a continuation of the work of last quarter, pre-lithiated PAA (LiPAA) binders have been evaluated in full cells with controlled NP ratios. The adhesive/cohesive strength of laminates was also evaluated by peeling tests. Secondly, the re-engineered poly (4-vinylbenzoic acid) or P4VBA binders have been evaluated in full cells and the cycled electrodes are analyzed. Thirdly, two electrolyte additives, N-Allyl-N,N-bis(trimethylsilyl)amine (NNB) and Tris(trimethylsilyl) phosphite (TMSPi), have been evaluated with Si-Gr composite anodes.

Results

Pre-lithiation of PAA binders: A new set of full cells have been fabricated with more reasonable NP ratios (ranging from 1.1 to 1.4) and a CAMP supplied cathode, $\text{LiNi}_0.5\text{Co}_0.2\text{Mn}_0.3\text{O}_2$ (NCM523, C-013A), was used to couple with Si-Gr composite anodes. The full cells were subjected to a standard testing protocol, containing three formation cycles at a nominal C/20 rate, a hybrid pulse power characterization (HPPC) test, ninety-two aging cycles at a C/3 rate, another HPPC test and three final cycles at a C/20 rate, for a total of 100 cycles with the cell voltage between 3.0-4.2 V. The specific capacity profiles are shown in **Figure 1**. The controlled NP ratios indeed afford a different view of full cell cycling. From **Figure 1**, the observed trend based on the average capacity is **PAA-2.1>PAA-4.2>PAA-6.0>PAA-4.8>PAA-7.0**, which is more consistent with the half-cell cycling results. Peeling test was used to assess the adhesive/cohesive strength of the electrode. As shown in **Figure 2**, the load profiles indicate that the increased lithiation of PAA decreases the cohesion in the matrix. This can be attributed to the reduced number of COOH groups that can esterify SiOH groups at the surface of Si particles, forming strong bonds between the polymer chains and the silicon particles. Overall, this study indicates that less pre-lithiation seems more beneficial to Si-Gr composite anodes.

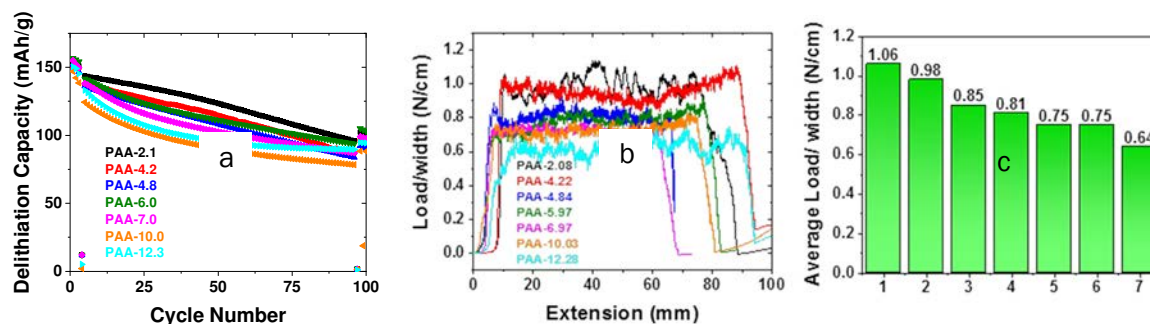


Figure 1. (a) Specific delithiation capacity profiles for NCM523/Si-Gr full cells containing lithiated PAA binders with different pH values. (b) The 180° peeling profiles for the Si-graphite electrode fabricated using lithiated PAA binders (pH values from Figure 1 given in the inset). (c) Average load/width with a range of 50 mm for Si-Gr electrodes.

Poly (4-vinylbenzoic acid) (P4VBA) binders: P4VBA binders have been designed by incorporation of arene rings into the PAA backbones, which are believed to enhance the mechanical properties. Those binders have shown improved cycling performance of Si-Gr half cells using NMP solvents during lamination. This quarter, we further evaluate them in full cells. As shown in **Figure 2**, three P4VBA binders with different molecular weights (MW) (Mn: 63.5K, 23.2K, 8.1 K for P4VBAA-1, P4VBA-2, and P4VBA-3, respectively) have been evaluated in full cells. The NP ratios are kept in the range of 1.1 to 1.2. The cycling tests are ongoing but based on what we have, it is clearly that high MW binder, P4VBA-1, can afford better cycling performance in the full cells.

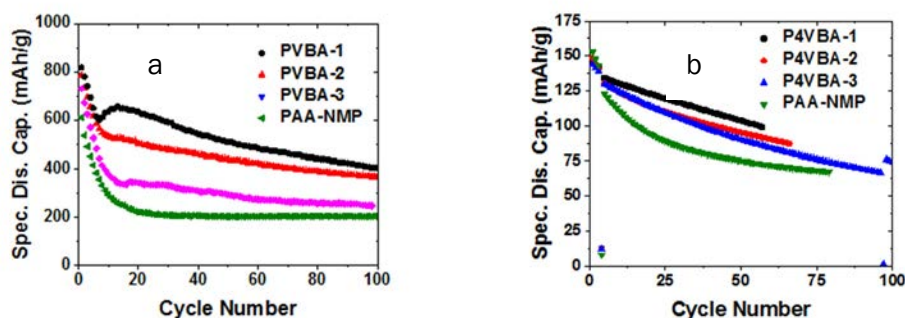


Figure 2. (a) Specific capacity profiles Si-Gr half cells (a) and NCM523/Si-Gr full cells (b) containing P4VBA binders with different molecular weights.

Electrolyte additives: Two electrolyte additives have been evaluated in Si-Gr half cells. **NNB** and **TMSPi** (see structure in **Figure 3**) have been reported to prompt a more sturdy SEI layers for lithium-ion batteries containing carbonaceous anodes. [2-3] Their ability of forming polymeric networks on electrode surface may also benefit the Si-Gr anodes. As shown in **Figure 3**, both additives show obvious improvement on the half-cell cycling with higher initial capacity and averaged capacity. For full cells, the cycling tests are ongoing and the cycling results so far are promising.

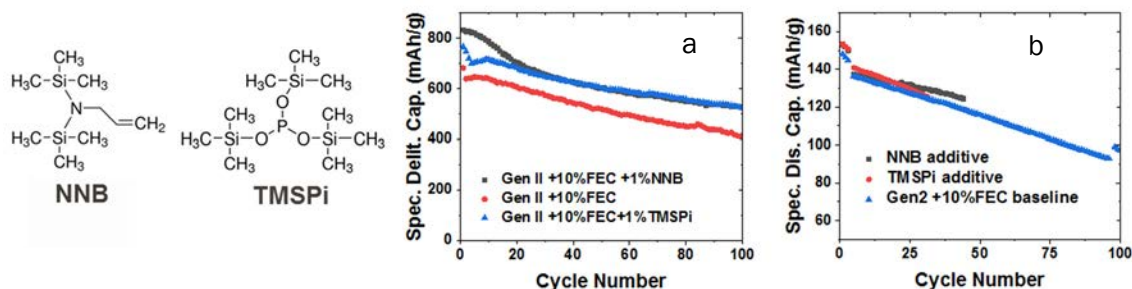


Figure 3. Chemical structures of NNB and TMSPi and specific capacity profiles Si-Gr half cells (a) and NCM523/Si-Gr full cells (b) containing 1 w% NNB or TMSPi additives.

Conclusions

This quarter we continue to work on binders and start to extend to electrolyte additives for Si-Gr composite electrodes. The full cell tests using LiPAA binders have been redone and the new results are more consistent with the half-cell data, which reveal that less pre-lithiation could be beneficial to Si-Gr anodes. We also tested P4VBA binders, a family of re-engineered PAA based binders, in full cells. The results are confirming the positive improvements that were observed in half cells. Finally, two electrolyte additives, **NNB** and **TMSPi** are being tested in half cells and full cells using Si-Gr anodes and preliminary results show great promise.

References

1. Hu, B.; Shkrob, I. A.; Zhang, S.; Zhang, L.; Zhang, J.; Li, Y.; Liao, C.; Zhang, Z.; Lu, W.; Zhang, L., The existence of optimal molecular weight for poly(acrylic acid) binders in silicon/graphite composite anode for lithium-ion batteries. *Journal of Power Sources* 2018, 378, 671-676.
2. Zheng, Q.; Xing, L.; Yang, X.; Li, X.; Ye, C.; Wang, K.; Huang, Q.; Li, W., N-Allyl-N,N-Bis(trimethylsilyl)amine as a Novel Electrolyte Additive To Enhance the Interfacial Stability of a Ni-Rich Electrode for Lithium-Ion Batteries. *ACS Applied Materials & Interfaces* 2018, 10 (19), 16843-16851.
3. Yim, T.; Han, Y.-K., Tris(trimethylsilyl) Phosphite as an Efficient Electrolyte Additive To Improve the Surface Stability of Graphite Anodes. *ACS Applied Materials & Interfaces* 2017, 9 (38), 32851-32858.

Probe the Relationships between Functional Electrolytes Structure and SEI Property for Si Materials

Gao Liu, Tianyue Zheng (Lawrence Berkeley National Laboratory)

Background

Electrolyte decomposition products play a critical role in the stabilization of the negative electrodes in lithium-ion batteries, as the negative electrode is operated outside the stability window of the electrolyte. The electrolyte decomposition products form insoluble SEI layer, which stabilizes the electrode and electrolyte interface. Silicon alloy material has large volume expansion and surface reactions with the electrolyte when it is electrochemically lithiated. When delithiated, the Si alloy volume shrinks and the surface area also decreases. This dynamic surface area changes cause excessive side reactions with the electrolyte. Moreover, some of the key electrolyte decomposition products are soluble in the electrolyte rather than solid precipitates. Surface coatings on Si materials by organic and ceramic have demonstrated improved surface stability towards electrolytes. Nano-sizing the Si materials can successfully prevent cracking of Si material. The Si particles are assembled by a functional polymeric binder to further improve the electrode stability in a composite electrode. We have demonstrated that both Si surface coating and functional binders can enhance cyclability of the Si based composite electrode. Surface coating on Si can prevent electrolyte interaction with the reactive surface and slow down the side reactions at the interface. Here, we propose to further reduce the Si surface reactivity by investigating electrolyte and additive functions to SEI formation and stabilization.

This project is aimed to gain a comprehensive understanding of electrolyte decomposition products to SEI property relationship, and to guide the design and synthesis of new electrolytes and additives for Si based materials. New electrolyte design with consideration of the SEI structure and functions on the Si materials can lead to enhanced Si performance over the traditional mixed carbonate based electrolyte. Designing organic molecules with preferred decomposition pathways during electrochemical process can lead to controlled SEI formation on Si surface.

Results

An effort to construct a bi-functional additive toolbox is underway. The bi-functional additive molecules have one reaction functional group to form coating on the surface of Si particles at low potentials, and another functional group to provide desired surface properties for the SEI layers. The reaction functional groups can also react with each other to form bulk polymer in a controlled organic chemistry environment. In this quarter, the methacrylate group is investigated as the reaction group, along with hydrophilic or hydrophobic functional groups (Figure 1). Four new additives in this series are identified and used. The first one is methylmethacrylate (MMA) molecule, which has a simple methyl group connected to the ester oxygen. The second one is butylmethacrylate (BuMA) with butyl moiety connected to the ester oxygen. The third one is dodecylmethacrylate (DoMA), which has an extended hydrophobic dodecyl group connected to the ester

oxygen. Both BuMA and DoMA are hydrophobic due to the alkyl moieties, with DoMA more hydrophobic. The fourth one is MATEGM, where triethyleneoxide monomethylether moiety connects to the methacrylate oxygen to make it more hydrophilic. The methacrylate reaction group can react with the Si surface at low potential. The hydrophilic and hydrophobic moieties can tune the properties of the Si surface layer.

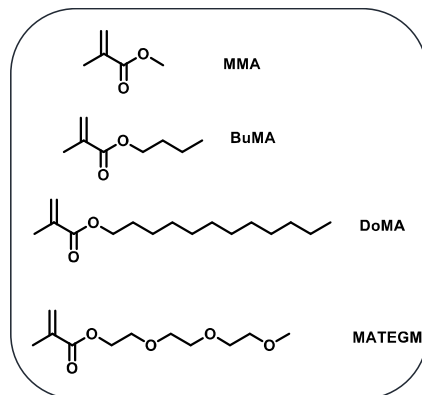


Figure 1. Methacrylate based additives

The electrolyte are formulated with 2% additives in a baseline electrolyte of 1M LiPF₆ in EC:EMC (3:7 by weight) solvent. These electrolytes are used in a coin type of testing cell. The cell has either graphite electrode or Si working electrode against lithium metal counter electrode with the formulated electrolytes. In order to understand the additive reactivity towards the working electrodes, the cells are cycled at C/25 current rate between 0.01V and 1V voltage window. The dQ/dV of the first lithiation step (C/25 rate) are plotted against the cell voltage (Figure 2). The electrochemical response towards the electrolyte additive effects is very consistent when tested against graphite electrodes (Figure 2a). The additives breakdown voltage shift from 1.2V to 0.9V, while the moieties on methacrylate oxygen get more bulkier from methyl to dodecyl functional groups. The baseline electrolyte without additive does not show any reactivities in this voltage window. The voltage of SEI formation due to the breakdown of bulk electrolyte around 0.8V also shows a systematic change due to the additives. The bulk electrolyte breakdowns are also shifted by 0.1V from baseline electrolyte without additive to the electrolytes with additives. The bulkier the additive functional groups, the larger the voltage shift towards the lower voltage. The bulkier groups delay the electrolyte breakdown on the graphite particle surface. However, the hydrophilic and hydrophobic effect between the DoMA and MATEGM additives is not differentiable in the case of graphite electrode based cells. When the electrolyte additives are used in a Si based electrode (Figure 2b), the additive reactivity is coupled with the Si surface oxide transformation between 0.5V and 1.5V, so the actual reaction groups reactivity on the Si surface in this voltage range is convoluted by the surface oxide transformation. Similar trend of delayed reactivity due to the bulkiness of the side chains can still be observable in Figure 2b, but less consistent than that using the graphite electrodes cell. However, DoMA shows stronger prevention of surface reaction than that of the MATEGM in case of Si based cells. DoMA additive also helps to push the lithiation to much a lower potential due to its hydrophobicity.

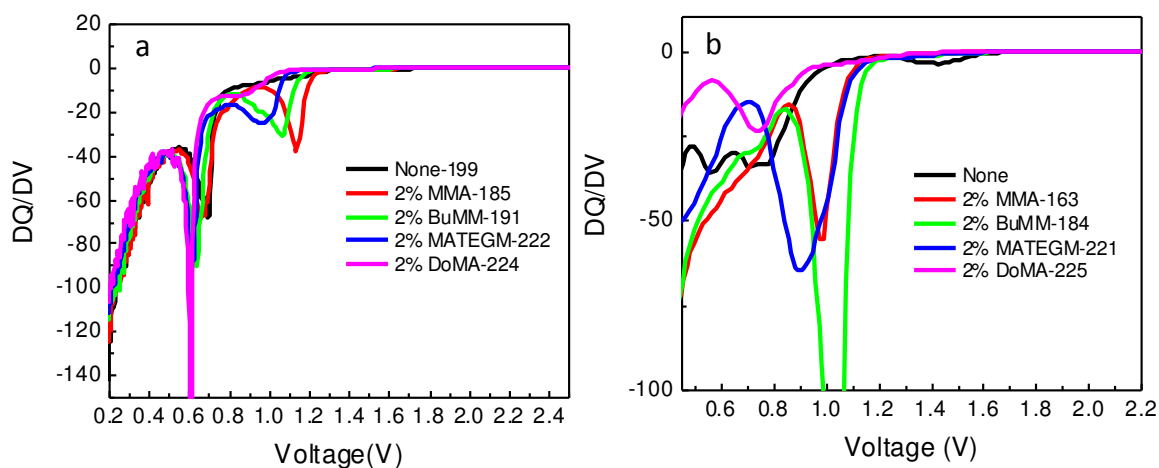


Figure 2. The dQ/dV curves of the first lithiation of the graphite (a) and Si electrode (b) based on different electrolyte additives. The counter electrode is lithium metal; the current density is C/25.; the baseline electrolyte composition is 1M LiPF₆ in EC:EMC (3:7 by weight); the baseline electrolyte performance is label as None, and other additives at 2% by weight and as labeled in the graph.

Conclusions

We have successfully identified a second group of bi-functional electrolyte additives with methacrylate as reaction group and a hydrophobic or hydrophilic moiety as functional side groups. The dQ/dV tests are performed with this group of additives, showing systematic reduction of the voltage of reaction based on the bulkiness of the functional groups on the additives. This effect is more consistent with graphite electrode than that with Si electrode. The hydrophobicity of the functional groups (Dodecyl group) drastically reduce the lithiation voltage with Si based electrode. The initial electrochemical characterizations are performed with lithium counter electrode cells. More systematic testing is being performed with full cells to fully characterize the additives' performance.

Silicon Surface Modification and Interaction

Taeho Yoon, Yanli Yin, Jasmine Melissa Wallas, Chunmei Ban (National Renewable Energy Laboratory)

Background

This project aims to develop a systematic understanding and synthesis of surface coating materials to chemically or physically change the surface of the silicon (Si) materials, in order to improve the interphase chemistry, conductivity, and mechanical integration in Si-based electrodes. Continuous decomposition of electrolyte on the silicon surface is one of the factors dictating the electrochemical performances of Si electrode. Tremendous efforts have been dedicated in our lab to stabilizing the surface: (i) depositing an artificial interface layer through atomic layer deposition (ALD) and molecular layer deposition (MLD); (ii) using a polymeric binder that mitigates electrolyte decomposition, and (iii) introducing electrolyte additives that sacrificially decompose to generate a protective film (e.g., FEC or VC). To study the fundamental roles of the surface species on the electrochemical and physical properties of the electrodes, we devoted FY 18 research to develop the liquid-phase deposition process to functionalize the silicon surface. The liquid-phase deposition are capable to explore various functional groups and can be applied for both laminated electrodes and the nanoparticles. The in-depth understanding from these studies will help establish effective mitigation to address the key challenges in Si-based electrodes; and develop strategies to deploy high-energy silicon alloys and composite electrode configurations in the full Li-ion cells.

Results

The work in this quarter has been focused on the chemical interaction of the surface functional groups with the electrolyte. As we previously reported, functional groups, herein $-\text{CH}_3$, $-\text{CF}_3$, and $-\text{COOH}$, which are found in the polymeric binding materials, have been selected and deposited on the surface of our Si (100) wafer electrodes. The illustration of surface treatment, chemical composition of SEI formed on the functionalized Si wafer, and electrochemical properties have been discussed in previous reports. Based on our electrochemical and impedance data, the coulombic efficiency of the fictionalized Si electrodes for the 1st cycle decreases in the order of $-\text{CF}_3$ (92.9%) > CH_3 (92.2%) > COOH (91.8%) > Pristine (90.9%), while the surface resistance at the end of lithiation period decreases in the order of $-\text{CH}_3$ (420 Ω) > Pristine (180 Ω) > $-\text{CF}_3$ (140 Ω) > $-\text{COOH}$ (100 Ω).

Here, this report presents the main work on the study of ion transport mechanism by using electrochemical impedance of the functionalized Si electrodes. Besides the Nyquist plots—usually used in electrochemical impedance spectroscopy (EIS), we introduce the Bode plots to better understand the ion transport in the functionalized Si electrodes. As aforementioned, the surface resistance of the $-\text{CH}_3$ functionalized electrode has a much larger resistance than that in the $-\text{COOH}$ functionalized electrode. Furthermore, a suite of in-situ EIS data of these two functionalized electrodes was measured during the lithiation and delithiation process.

A representative 1st-cycle voltage profile of Si wafer is provided in Fig. 1a. The in-situ EIS was conducted by using a 3-electrode cell configuration, without disturbing the electrochemical process. GEN2 electrolyte with 10% FEC was used for all of experiments. EIS was measured at the specific potential (A-E), as illustrated in Fig. 1a. The SEI formed on $-\text{CH}_3$ (or $-\text{COOH}$) surface is denoted as SEI- CH_3 (or SEI- COOH) hereafter. In Figs. 1b and c, the Nyquist plots visualize the evolution of surface resistance during the lithiation and delithiation process. The semi-circle in the high-frequency range of the Nyquist plot reflects the resistance of SEI formed on surface of the functionalized Si electrodes. The SEI resistances of both SEI- CH_3 and SEI- COOH are quite stable during both cathodic and anodic process; while the SEI resistance of the SEI- CH_3 is about 4 times larger than that of SEI- COOH . Despite the SEI resistance is distinctive in the Nyquist plots, the charge transfer resistance is undetectable in these Nyquist plots. The semi-circle responding to the charge transfer resistance should appear in the mid-frequency range, however has been significantly overlapped with either the SEI resistance measured in the high-frequency range or Warburg diffusion resistance measured in the low-range frequency. Although Nyquist plots can provide an apparent convenience for reading resistances, the plots can present only limited information.

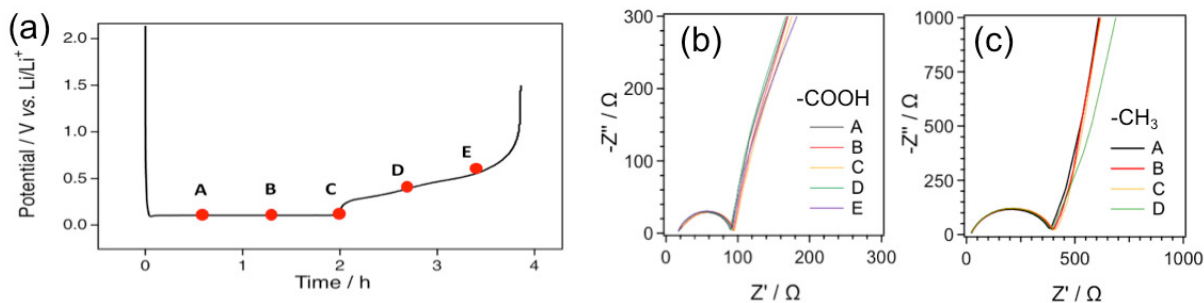


Figure 3. (a) A representative voltage profile of Si wafer electrode. (b) and (c) Nyquist plots of SEI- CH_3 and SEI- COOH . EIS measurements were conducted at specific state of lithiation and delithiation marked by the red circles in (a).

To complement the Nyquist plots, Bode plot is used and presented in Fig. 2, in which the phase angle is plotted versus frequency. The Bode plot shows the frequency dependency, thus it is easy to distinguish the individual electrochemical response that has a different time constant. The high-frequency region from 10^6 ~ 10^1 Hz is related to the SEI resistance. The peak centered at 10^4 Hz reflects the mobility of lithium ions in the SEI formed by FEC decomposition, which was observed for both functionalized electrodes. However, the plot

from the SEI-COOH has a shoulder in the frequency range between $10^6 \sim 10^4$ Hz, whereas the plot from the SEI-CH₃ shows a little bit longer tail in the frequency range between $10^4 \sim 10^1$ Hz. Because the COOH groups on Si wafer can react with electrolyte, leading the formation of an interlayer composed of lithium carboxylate between the Si electrode and the FEC-driven SEI. The reaction is summarized as $(-\text{COOH} + \text{Li}^+ + \text{e}^- \rightarrow \text{COOLi} + \text{H}_2)$. [1] The shoulder of SEI-COOH is likely to reflect the mobility of lithium ions passing through -COOLi layer. As compared to the interlayer formed on the -COOH functionalized electrode, the interlayer between the -CH₃ functionalized electrode and the SEI has a higher resistance, reflected as the long tail in the lower frequency range. It is clear that both functionalized electrodes have a multi-layer structure on the surface of the electrode, although the resistance is very different based on their interaction with the electrolyte. The lithium-ion mobility is higher in the -COOLi layer than the -CH₃-incorporated layer.

The charge transfer reaction can be identified as a separated semi-circle in Nyquist plots. However, the semi-circle can be sometimes largely overlapped with Warburg resistance for the wafer electrode, as shown in Fig. 1b. Using Bode plots, as displayed in Fig. 2a, the charge transfer behavior can be detected as a shoulder-like peak in the mid-frequency range, $10^1 \sim 10^{-1}$ Hz. Along with the lithiation, the charge transfer resistance becomes smaller for the lithiated silicon electrodes. Therefore, the peak becomes invisible at the end of lithiation period, denoted as C. During delithiation, the peak become visible again. Regarding the SEI-CH₃, the charge transfer resistance is relatively small, which has been significantly overlapped with Warburg resistance. The information collected by both Nyquist and Bode plots implies (i) that the SEI formed on -COOH has a smaller SEI resistance—higher lithium ion mobility in the SEI layer, but higher charge transfer resistance than that in the SEI-CH₃. We think that the charge transfer resistance can provide the information related to the lithium-ion transfer at the interface between SEI and the electrode, as well as the solvation/desolvation process at the interface of electrolyte/SEI. More analysis is planned to better understand the charge transfer resistance, in order to provide a guidance for developing efficient coating materials. We expect that this work could provide not only an insight into designing novel surface coating layers but also a methodology for investigating impact of surface functional groups

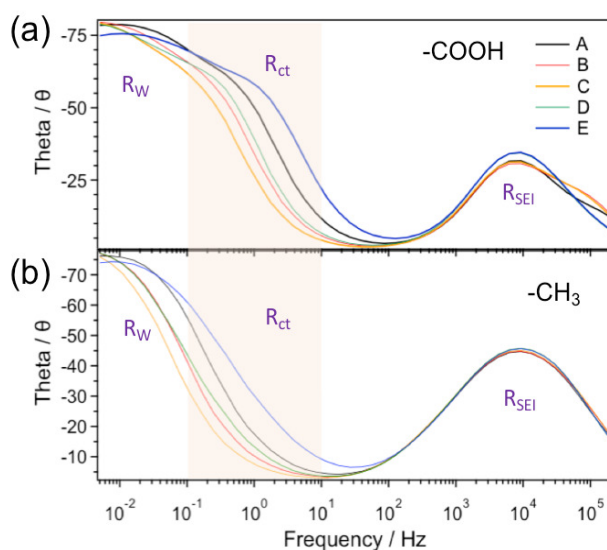


Figure 4. Bode plots of silicon electrodes functionalized by (a) -COOH and (b) -CH₃.

Conclusions

Electrochemical properties of the SEI formed on the functionalized Si wafers were investigated by using EIS. During lithiation and delithiation, quasi in-situ impedance spectra were obtained by using a unique 3-electrode

cells. Ion transport mechanism has been studied by complementing Nyquist plots with Bode plots. The SEI resistance and the charge transfer resistance of both SEI-COOH and SEI-CH₃ were interpreted thoroughly and compared. The EIS results indicate that (i) those two SEIs have a multi-layer structure. The surface functional groups have also been involved in formation of the SEI layers. (ii) the SEI resistance of the SEI-COOH layer is smaller than that of the SEI-CH₃ layer, but the SEI-COOH shows larger charge transfer resistance. For convincing the SEI structure proposed based on EIS data, the chemical structures of both SEI will be analyzed by using XPS or NR depth profiling. Correlating the chemical structure of SEI and its EIS response would provide effective paths to engineer the Si surface.

References

1. C.C. Nguyen, T. Yoon, D.M. Seo, P. Guduru, B.L. Lucht, ACS Appl. Mater. Interfaces 8 (2016) 12211–12220.

Interfacial Modification of Si Anode for High Energy Li-ion Battery

John Zhang (Argonne National Laboratory)

Background

In this quarter, we continue to research the surface modification of silicon particles by electrochemical approach and organic synthesis approach. The former is to design new electrolyte/additive that could chemically/electrochemically decomposes and deposits on the lithiated Si surface forming a resilient SEI layer that stabilizes the interfacial reactivity of Li_xSi and electrolyte. Another approach is to functionalize the surface of Si particles through organic silane chemistry forming an artificial SEI for improved performance.

Results

1. Fluorinated Carbonates Electrolytes.

Last quarter, we have formulated and screened a couple of fluorinated electrolytes for Si/graphite composite anode using an expedited testing protocol - 3 C/20 formation cycles, 100 cycles with C/2 rate (theoretical value) with a cutoff voltage of 0.05-1.5 V. Under these testing conditions, the baseline electrolyte Gen 2 + 10% FEC showed a very low capacity (< 300 mAh/g) after C/20 formation cycles and suffered from rapid capacity fade with cycling; however, the fluorinated electrolyte 1.0 M LiFSI FEC/FEMC (5/5 in volume) showed much higher capacity (500 mAh/g) and cycling stability. The improved stability is contributed from the synergetic effect of the LiFSI salt and the fluorinated solvents since either the same LiFSI salt dissolved in the traditional solvents EC/EMC or the same LiPF₆ salt dissolved in the fluorinated carbonates FEC/FEMC showed the worse performance. In this quarter, the cycling performance under normal testing protocol - 3 C/20 formation cycles, 100 cycles with C/3 rate (based on the capacity from the formation cycle) with a cutoff voltage of 0.01-1.5 V - were evaluated and the results were shown in Figure 1. The baseline electrolyte suffered from a dramatic capacity drop at the 40th cycle. In contrast, the 1.0 M LiFSI FEC/FEMC (5/5) electrolyte delivered very high initial capacity (700 mAh/g) without the activation process. When switched salt from LiFSI to LiPF₆, an activation process was observed and capacity was stabilized at relatively low value (500 mAh/g) (red line).

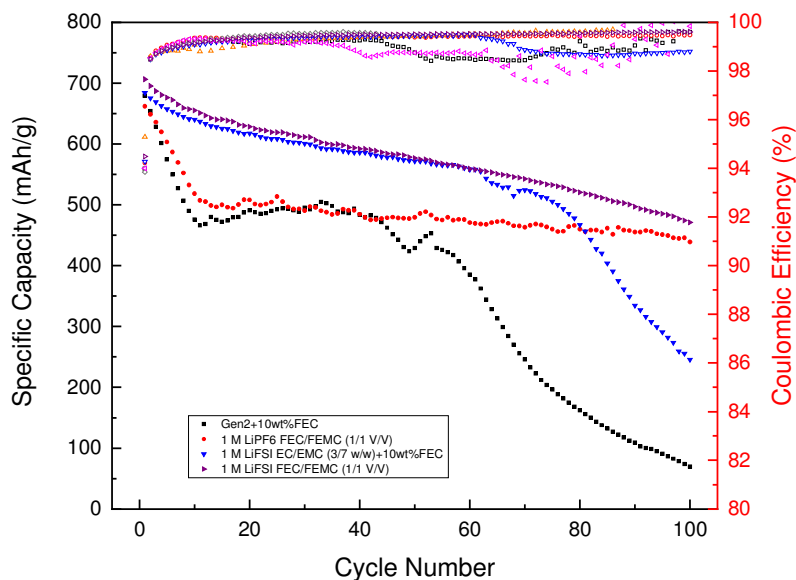


Figure 1. (a) Capacity retention and Coulombic efficiency of Si-graphite/Li cells with baseline electrolyte Gen 2+10% FEC, 1.0 M LiPF₆ FEC/FEMC (5/5), 1.0 M LiFSI EC/EMC (3/7 in weight) + 10% FEC and 1.0 M LiFSI FEC/FEMC (5/5). (C/3 for charge and discharge, the cutoff voltage is 0.01-1.5 V).

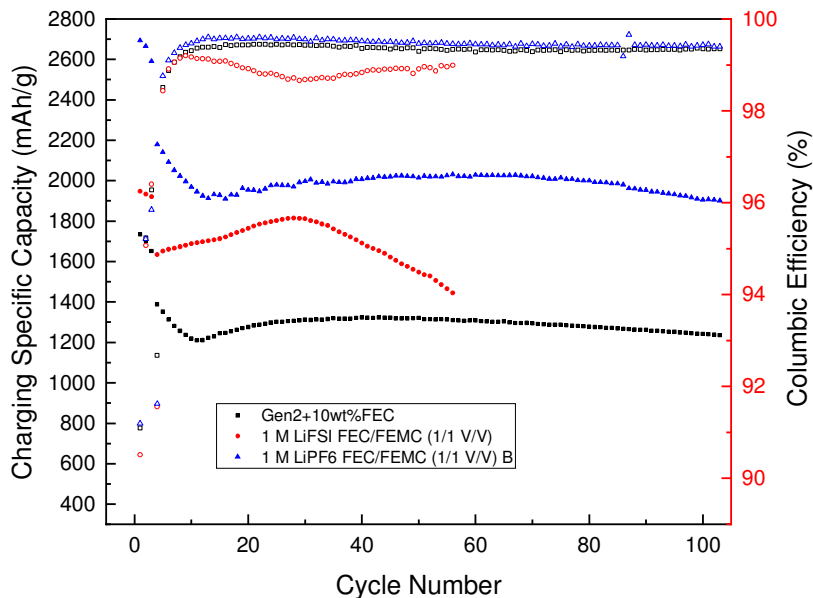


Figure 2. Capacity retention and Coulombic efficiency of Si/Li cells with baseline electrolyte Gen 2 + 10% FEC, 1.0 M LiPF₆ FEC/FEMC (5/5) and 1.0 M LiFSI FEC/FEMC (5/5). (3 C/20 formation cycles, 100 C/3 cycles (C/3 based on the capacity from formation cycle), the cutoff voltage is 0.01-1.5 V).

To distinguish the impact of the electrolyte on Si and graphite, anode with 100% Si as active material was fabricated with 70.7% NanoAmor Si (70-130 nm), 9.4% Timcal C45 and 19.9% LiPAA as binder. Under this testing condition, the 1.0 M LiPF₆ FEC/FEMC (5/5) electrolyte showed the best performance in terms of capacity and capacity retention as shown in Figure 2 indicating the best performing electrolyte 1.0 M LiFSI FEC/FEMC (5/5) for Si/graphite anode originates from the superior passivation capability of LiFSI on the graphite active material (73wt% in the anode composition).

2. Si Particle Surface Functionalization

In this quarter, new epoxy-containing functional silanes were designed and synthesized as shown in Figure 3. The introduction of the repeating ethylene oxide (EO) group on the silane functional group is targeted to facilitate the Li⁺ transport at the Si and electrolyte interface. EO repeating units have strong chelating strength with Li⁺ providing a feasible pathway for mass transfer. A series of silanes with different number of EO repeating units have been synthesized. The ¹H- and ¹³C-NMR spectra of the representative product epoxy-Di(EO)-triethoxysilane was shown in Figure 4. The electrochemical performance of these surface functionalized silicon particles will be evaluated and updated in the next quarter.

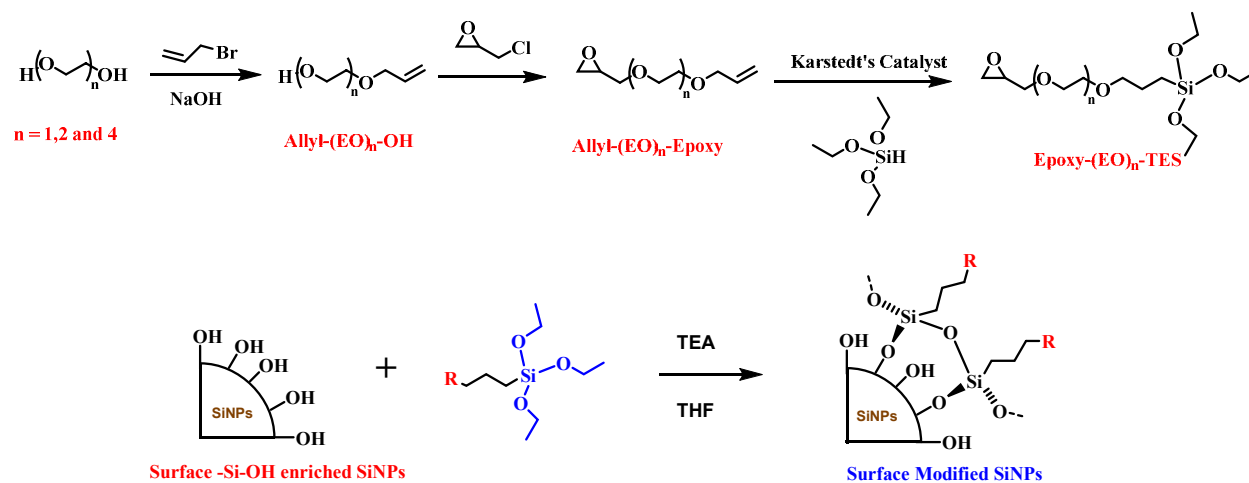


Figure 3. Synthetic routes for the epoxy-(EO)_n-triethoxysilane and its attachment to Si particle surface via the condensation reaction catalyzed by triethyl amine (TEA).

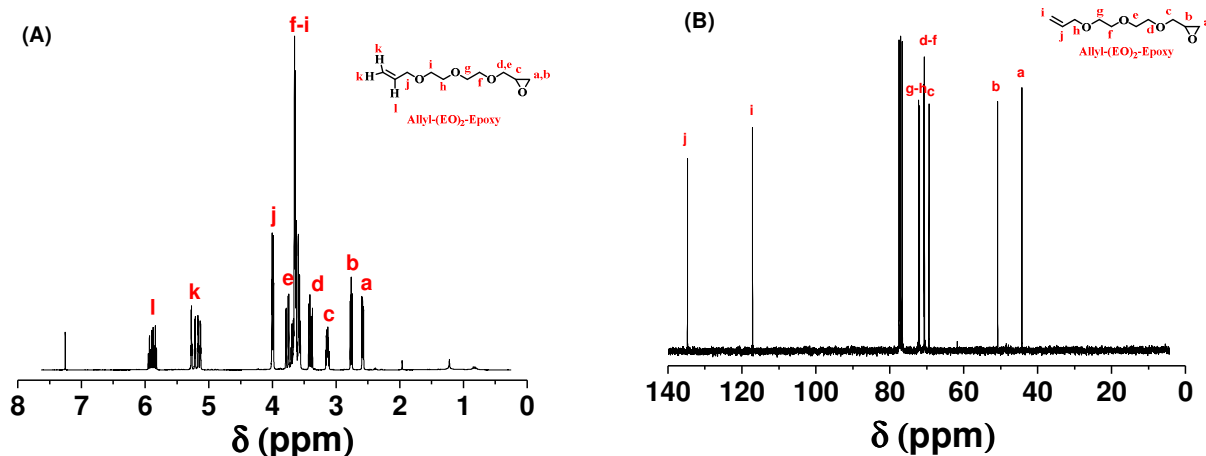


Figure 4. $^1\text{H-NMR}$ (left) and $^{13}\text{C-NMR}$ (right) spectra for the representative epoxy-Di(EO)-triethoxysilane.

Development of High Energy Metals

Wei Tng (Lawrence Berkeley National Laboratory)

Background

Thin films with the absence of binder and conductive carbon additive offers the opportunity to enable the effective characterization of solid-electrolyte interphase (SEI) formation and evolution upon electrochemical cycling. It is also of importance to evaluate and compare the electrochemical performance of Si-Me (Me is metal) thin films and bulk Si-Me that is to be produced by splat quenching method. Before the synthesis of Si-Sn thin films, we initially focused on the synthesis of Si thin films by magnetron sputtering method in this quarter. Physical and electrochemical properties of the as-produced Si films were investigated using X-ray diffraction (XRD), scanning electron microscopy (SEM), energy-dispersive X-ray spectroscopy (EDS), and electrochemical methods to identify the optimal synthesis condition.

Results

Si thin films were deposited onto Cu foils of 16 μm thickness by DC magnetron sputtering using a 4-inch p-type Si target (Kurt J. Lesker, 99.999% purity). Cu foils were fixed on the 4-inch Si wafer during the deposition. The base pressure before the deposition is 2×10^{-5} torr, the Ar flow during deposition is 7.5 sccm to maintain a chamber pressure of 1.4×10^{-2} torr, and the power is 250 W. All the Si films were subsequently stored under vacuum to prevent air exposure. Coin cells were assembled using the Si films deposited on Cu foils (1.6 cm^2) as the working electrodes, Li metal foil as the counter electrode, and 1 M LiPF_6 in ethylene carbonate (EC)-diethyl carbonate (DEC) (50: 50 wt%) as the electrolyte. The cells were cycled between 1.5 and 0.01 V at C/20 based on the experimental capacity. Cyclic voltammetry (CV) was carried out between 2 and 0.01 V at a scan rate of 0.1 mV/s.

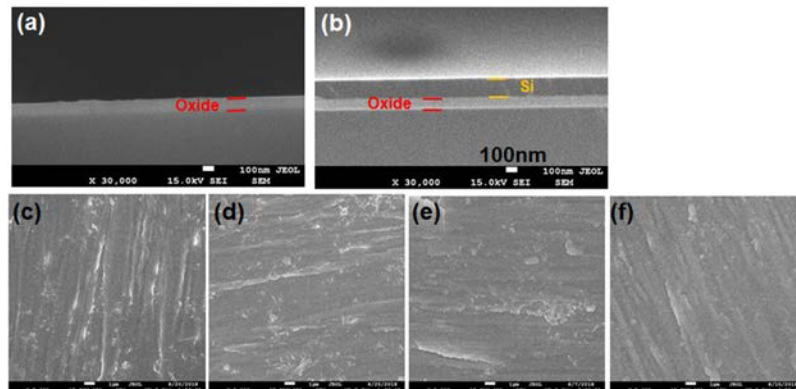


Figure 6 Cross sectional SEM image of Si wafer with 100 nm oxide (a) before and (b) after Si deposition for 20 min, and SEM image of (c) Si-5, (d) Si-10, (e) Si-20 and (f) Si-30 film.

Four films were prepared by depositing Si on Cu foil for 5, 10, 20 and 30 min, therefore, denoted as Si-5, Si-10, Si-20, and Si-30, respectively. In order to determine the deposition rate, Si film produced by 20 min deposition was also conducted on the Si wafer with 100 nm oxide on the surface to survey the cross section of the Si wafer after deposition *via* SEM. Figure 1a, b show the cross sectional SEM images of the Si wafer before and after Si deposition for 20 min. A layer of 100 nm oxide is clearly present on the Si wafer before deposition (Figure 1a), meanwhile, a layer of Si appears on the top of the oxide layer after the deposition. The thickness of the deposited Si is determined to be ~ 160 nm for Si-20 and the deposition rate is calculated to be ~ 8 nm/min. Therefore, the estimated thickness of Si-5, Si-10, and Si-30 is 40, 80, and 240 nm, respectively. SEM images of the Si thin films (Figure 1c-f) display similar morphological features, the surface roughness mainly originating from Cu foil. The EDS elemental distribution is presented in Table 1, showing a high consistency in O content and its independence of the Si deposition time. More importantly, Si content almost shows a linear correlation with the deposition time, suggesting a reliable control of film thickness *via* deposition time. Of note, all Si films display amorphous feature by XRD.

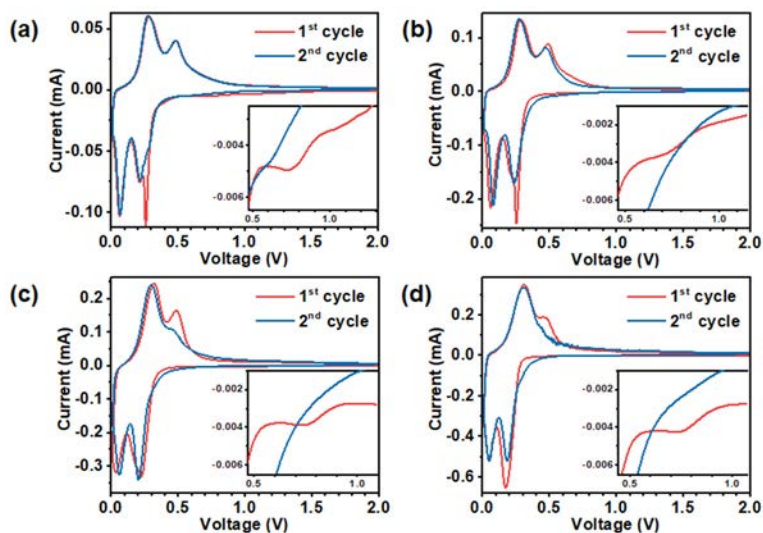


Figure 5 CV curves of (a) Si-5, (b) Si-10, (c) Si-20, and (d) Si-30 film during the first two cycles.

Figure 2 presents the CV curves of the as-produced Si films during the first two cycles. The corresponding lithiation/delithiation capacity and coulombic efficiency (CE) are summarized in Table-1. The small cathodic peaks at $\sim 0.7 - 0.8$ V are attributed to electrolyte decomposition and SEI formation during the 1st cycle (insets in Figure 2e-f). Except Si-5 sample, the measured current in this voltage range remains around -0.004 mA, independent of the Si film thickness. Meanwhile, all the films demonstrate typical lithiation of amorphous Si (a-Si), leading to the formation of amorphous Li_xSi (a- Li_xSi) at $\sim 0.2 - 0.3$ V, whereas all anodic curves show two broad peaks at ~ 0.3 and 0.5 V, corresponding to the Li extraction from a- Li_xSi . As summarized in Table-1, Si-5 electrode seems an outlier compared to the other three samples, which demonstrate a good consistency between lithiation/delithiation capacity and film thickness (film deposition time), as well as a similar initial CE of $\sim 82\%$. Detailed physical characterization on the as-produced Si films is underway to identify an optimal condition to produce Si film.

Table-1: EDX Elemental distribution, lithiation/delithiation capacity, and CE of the Si films prepared under different deposition time.

Deposition time (min)	Si (wt%)	O (wt%)	Cu (wt%)	1 st lithiation (mAh)	1 st delithiation (mAh)	1 st CE (%)	2 nd lithiation (mAh)	2 nd delithiation (mAh)	2 nd CE (%)
5	4.44	2.76	92.80	0.0853	0.0611	71.63	0.0680	0.0611	89.85
10	8.63	2.49	88.88	0.1364	0.1122	82.26	0.1202	0.1137	94.59
20	15.80	1.69	82.51	0.2720	0.2220	81.62	0.2326	0.2110	90.71
30	27.16	2.17	70.67	0.3590	0.2949	82.14	0.2977	0.2895	97.25

Conclusions

Si films with the thickness ranging from a few tens to a few hundred nanometers were synthesized by DC magnetron sputtering. The amount of deposited Si is directly proportional to the deposition time. The as-produced films are subjected to additional characterization to evaluate the cycling performance and verify the oxide content, therefore, determine the optimal synthesis condition for Si film. In the next quarter, we will prepare Si-Sn films to evaluate its physical and electrochemical performance. The optimal Si and Si-Sn films will be used to study the chemical and electrochemical activities towards different electrolytes.

Si Anodes with Extended Cycle Life and Calendar Life

Ji-Guang Zhang, Xiaolin Li (Pacific Northwest National Laboratory)

Background

Nano Si or highly porous structured Si has been widely used to avoid pulverization of Si particles during cycling process. However, large surface area of nano Si or micron sized porous Si may also lead to a continuous reaction between lithiated Si and electrolyte. As a result, this reaction may lead to continuous growth of SEI layer and increase of cell impedance. Another possible degradation mechanism is the cross talk between Si anode and cathode. The mitigation of dissolved Mn in cathode may poison Si anode; FEC additive which is highly effective in forming a stable SEI layer on Si may form a detrimental cathode electrolyte interface (CEI) on cathode surface which also leads to impedance increase. Therefore, minimize the surface area of Si and find a stable electrolyte additive are critical for long term stability of Si based Li-ion batteries.

In this project, we will enhance the cycle life and calendar life of Si based Li-ion batteries by designing a stable porous Si structure and develop an artificial SEI layer coated on the surface of porous Si particles. A more stable electrolyte additive or solvent mixture will be developed to minimize the detrimental effect of FEC

currently used in Si based Li-ion batteries. The degradation mechanism of Si anodes during shelf storage will be systematically investigated. New insight on these mechanisms and the new approaches developed in this work will speed up the deployment of high energy Li-ion battery with Si-based anodes and increase market penetration of EVs and PHEVs as required by DOE/EERE.

Results

In this quarter, the long-term cycling performance of NMC532||Si/Gr full cells (both cathodes and anodes are provided by CAMP Facility of ANL) have been investigated using novel electrolyte and additives that can improve the stability of the SEI on the electrode-electrolyte interface. The cell tests were done following the standard protocol recommended by ANL. The electrolyte amount added in the 2032 coin cells used in these tests was controlled at $\sim 45 \mu\text{l}$. We have tested more than 20 kinds of additives including Tris(trimethylsilyl) borate (TMSB), Succinonitrile (SN), Fumaronitrile (FN), Tris(trimethylsilyl) phosphite (TMSP), Diphenyldimethoxysilane (DPDMS), Prop-1-ene-1,3-sultone (PES). The performance were compared side-by-side to the baseline electrolyte of 1.2M LiPF_6 in EC: EMC (3:7, by weight) with 10% FEC (referred to E-control). Table 1 and Figure 1a below showed the preliminary results of the additives having improved performance. TMSB and SN additives can effectively improve the first cycle Coulombic efficiency (FCE), while the cycling performance is comparable to that using baseline electrolyte. TMSP and PES improve the cycling stability for the first 50 cycle. DPDMS stands out as the best additive with slightly increased the cycling performance after 100 cycles.

In another effort, LiFSI-based electrolyte was also evaluated for NMC532|| Si/Gr full cells. Preliminary results in Figure 1b shows better Coulombic efficiency and cycling stability compared to the baseline electrolyte. Long term performance will be reported later. In next quarter, new electrolyte and additives will be further investigated using the standard Si anodes from CAMP. In addition, nano-structured Si will be further improved to further extend the cycle life and calendar life of Si anode.

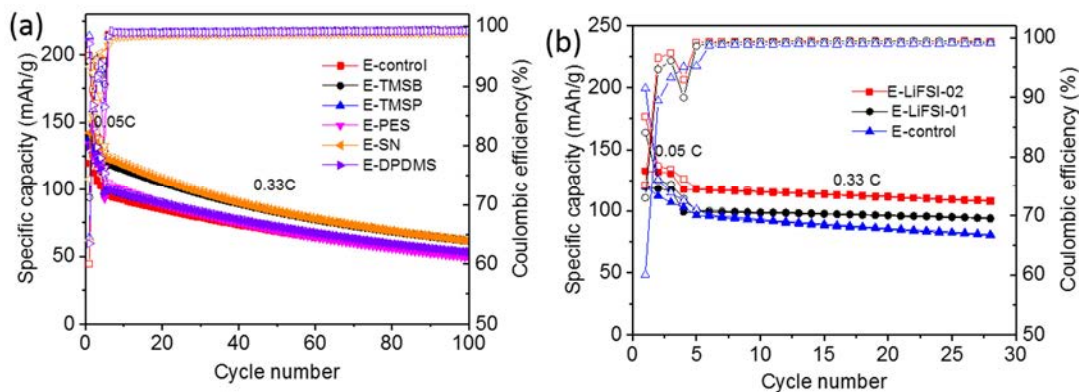


Figure 1. Cycling performance of NMC532|| Si/Gr full cell using baseline electrolyte (1.2M LiPF_6 in EC/EMC-10% FEC) with different additives (a) and new electrolyte using LiFSI salt (b).

Table-1: Representative values for the first cycle efficiency and capacity retention (50th and 100th cycle) of NMC532 || S/Gr full cell

Experimental table-cycle test					
#	Electrolyte	Additive Concentration	FCE	Retention at 50 cycles (%)	Retention at 100 cycles (%)
Baseline	1.2M LiPF ₆ in EC/EMC-10% FEC		60-65	71.2	53.4
1	Plus, TMSB	1 wt %	71-72	71.1	50
2	SN	1 wt %	74-75	67.1	47.9
3	FN	1 wt %	67	61.4	42.7
4	TMSP	1 wt %	65	72.6	52.1
5	PES	1 wt %	64	74.3	52.8
6	DPDMS	1 wt %	64	74	54.5

Conclusions

The nitrile and borate electrolyte additives of SN, FN and TMSB can improve the initial Coulombic efficiency. The silane-based electrolyte additive of DPDMS helps to improve the capacity retention. In addition, preliminary results showed that the full-cells containing LiFSI-based electrolytes demonstrated higher Coulombic efficiency and improved cycling performance.

Lithium Inventory

C. S Johnson and W. M Dose (Argonne National Laboratory)

Background

Maintaining a complete lithium inventory during cycling is critical to meet the cycle life targets of advanced Li-ion batteries. Lithium inventory is depleted in the cell via a number of processes, such as solid electrolyte interphase (SEI) forming reactions, lithium trapping, active material loss, *etc.* A relatively large amount of lithium is irreversibly lost during the first cycle, mostly due to SEI formation. For graphite anodes, the SEI film passivates the electrode and protects it from further Li-consuming reactions. However, in Si-containing electrodes the large volume changes associated with (de)alloying reactions during cycling cause the exposure of fresh surfaces to the electrolyte. Further reactions take place to passivate these new surfaces, giving rise to a mechanism for ongoing depletion of the lithium inventory in every cycle.

We have proposed various strategies to introduce additional lithium to the cell to account for the first cycle irreversible capacity (summarized below). However, does the placement of this lithium reserve (*e.g.*, on the cathode or anode) have an impact of the subsequent cycling behavior? In this quarter we focused on answering this question by consideration of the irreversible capacity both while the lithium reserve is present and after it is exhausted.

Results

Our previous work has addressed Li inventory through a number of avenues, as summarized briefly here.

- The capacity fade of the Si-graphite electrode was tracked using a **capacity over-sized LiFePO₄ cathode in a diagnostic cell**. With essentially limitless Li inventory the intrinsic capacity fade was tracked over hundreds of cycles, without limitations from Li metal in a half cell.
- **Introducing lithium inventory to the cell #1.** To date we have investigated in detail the synthesis and electrochemistry of Li₅FeO₄ as a prelithiation source. We are currently working towards a blended LFO-NMC cathode to understand the cross-reactivity, impedance changes, and capacity changes in the resultant electrode.
- **Introducing lithium inventory to the cell #2.** Overlithiated NCM, *i.e.*, Li_{1+x}NCM523O₂, was found to be a viable way to introduce lithium to the cathode with minimal weight increase and no residual byproduct. However, we reported in quarter one that the electrochemical cycling stability of overlithiated NCM is compromised, likely a result of the irreversible anisotropic structural changes. Work is ongoing to assess the nature of the irreversibility and we are developing strategies to minimize its impact.
- **Introducing lithium inventory to the cell #3.** Last quarter we reported that the 5 V spinel cathode, or Li_{1+x}Ni_{0.5}Mn_{1.5}O₄, could be further lithiated via an ammonia-based chemical lithiation reaction. This material was paired with a Si-graphite anode in a full cell. The excess lithium is released during the first charge and accounts for the first cycle irreversible capacity loss. Subsequent cycling shows a higher capacity and similar fade rate compared to the baseline, unlithiated cathode.

In this quarter, we investigate the impact of the placement of the lithium reserve. In our previous work, the lithium reserve was initially located on the cathode and was released to the anode on the first charge. However, direct lithiation of the Si-graphite anode is also possible by electrochemical means. Thus, one objective from Li inventory is to suggest the ideal location for the lithium reserve. Here we design experiments using a LiFePO₄ diagnostic cathode together with capacity limited cycling to understand the impact of the lithium reserve location on the cycle behavior, and particularly its impact (if any) on the per cycle irreversible capacity. The cycling performance of Si-graphite/LiFePO₄ cells with the lithium reserve on the cathode and anode are shown in Figure 1a and 1b, respectively.

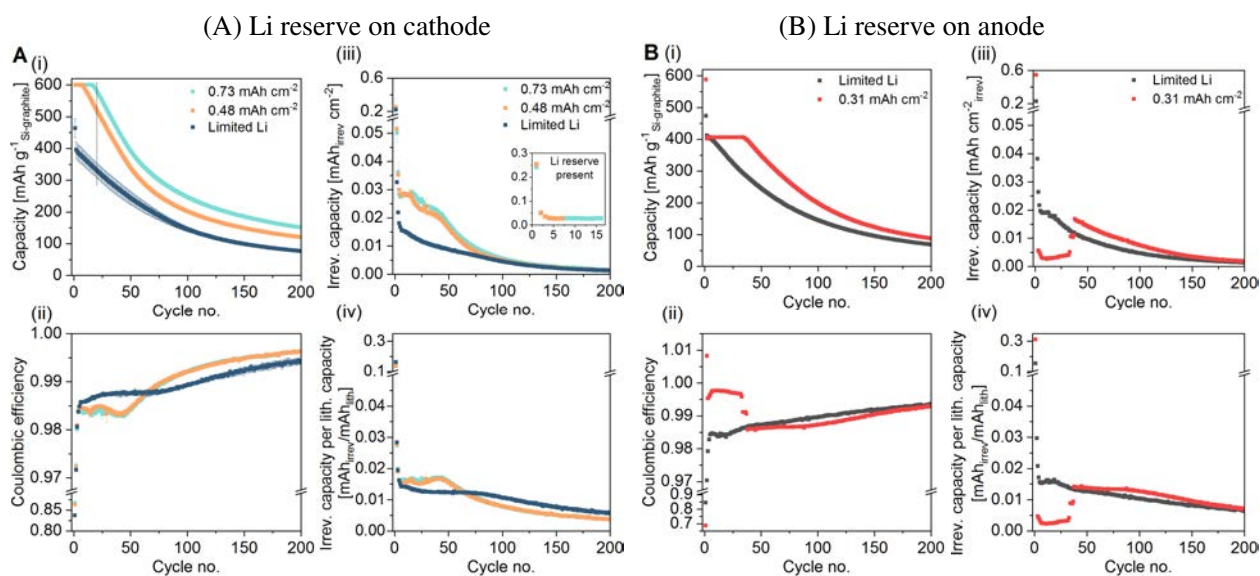


Figure 1. Si-graphite/LiFePO₄ cells with Li reserve on (A) the LiFePO₄ cathode and (b) the Si-graphite anode. In each figure (i) shows the capacity fade over 200 cycles, (ii) the Coulombic efficiency, (iii) the irreversible capacity per cycle, and (iv) the irreversible capacity normalized to the lithiation capacity.

These results indicate that a lithium reserve on the cathode or anode acts to delay capacity fade. In addition, the irreversible capacity per cycle is dependent on the lithiation capacity (*i.e.*, extent of lithiation of Si-graphite). From cycle 35 onwards, once the lithium reserve is exhausted, the irreversible capacity per lithiation capacity is $\sim 0.01 \text{ mAh}_{\text{irrev}}/\text{mAh}_{\text{lith}}$ irrespective of whether the lithium reserve is on the cathode or anode. Due to the nature of the experiment, the Li reserve present on the anode masks the true Coulombic efficiency and irreversible capacity giving artificially high and low values, respectively, in the first 34 cycles. Further work is required to understand the rate of Li inventory loss while the Li reserve is present.

Conclusions

A LiFePO_4 diagnostic cathode was paired with a Si-graphite anode to determine the impact of Li reserve placement in the full cell. After the Li reserve was consumed, the normalized irreversible capacity (per lithiation capacity) was determined to be equal whether the reserve was on the cathode or anode. These results suggest that the placement of the Li reserve does not affect the rate of capacity loss once the reserve is exhausted, leaving a wider scope for different sources of Li inventory to be utilized. Further work is required to probe the rate of capacity loss while the Li reserve is present. Additionally, we plan to use a three-electrode setup to differentiate Li loss from other sources of irreversible capacity, and relate this to the Si-graphite electrode state of charge.

References

W. M. Dose, V. A. Maroni, M. J. Piernas-Munoz, S. E. Trask, I. Bloom, and C. S. Johnson, Assessment of Li-inventory in cycled Si-graphite anodes using LiFePO_4 as a diagnostic cathode, *J. Electrochem. Soc.*, submitted.